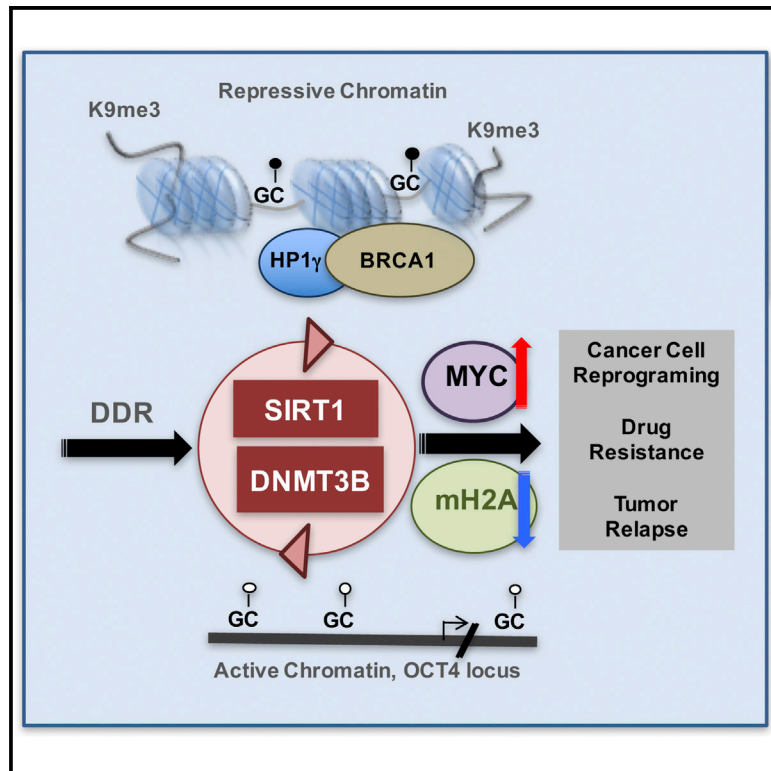Article

DNA Damage Signaling-Induced Cancer Cell Reprogramming as a Driver of Tumor Relapse

Graphical Abstract

Authors

Doria Filipponi, Alexander Emelyanov, Julius Muller, Clement Molina, Jennifer Nichols, Dmitry V. Bulavin

Correspondence

dmitry.bulavin@unice.fr

In Brief

The work by Filipponi et al. supports a model in which many, if not all, cancer cells independent of hierarchical organization can be challenged by DNA damage-induced signaling to undergo a series of epigenetic reprograming events, including reactivation of OCT4, ultimately contributing to development of drug resistance and tumor relapse.

Highlights

- DDR signaling induces DNA demethylation at defined loci, including OCT4 and NANOG

- macroH2A counterbalances a DDR-signaling-induced activation of OCT4

- MYC and SOX2 cooperate with DDR signaling to activate OCT4 transcription

- OCT4 reactivation contributes to cancer drug resistance and tumor relapse

CellPress

Molecular Cell

Article

CellPress

DNA Damage Signaling-Induced Cancer Cell Reprogramming as a Driver of Tumor Relapse

Doria Filipponi,[1] Alexander Emelyanov,[1] Julius Muller,[2] Clement Molina,[1] Jennifer Nichols,[3] and Dmitry V. Bulavin[1,4,5,*]

[1]Institute for Research on Cancer and Aging of Nice (IRCAN), INSERM, Université Côte d'Azur, CNRS, Nice, France
[2]The Jenner Institute, University of Oxford, Old Road Campus Research Building, Roosevelt Drive, Oxford OX3 7DQ, UK
[3]Wellcome Trust - Medical Research Council Cambridge Stem Cell Institute, University of Cambridge, Tennis Court Road, Cambridge CB2 1QR, UK
[4]Centre Antoine Lacassagne, Nice, France
[5]Lead Contact
*Correspondence: dmitry.bulavin@unice.fr
https://doi.org/10.1016/j.molcel.2019.03.002

SUMMARY

Accumulating evidence supports the role of the DNA damage response (DDR) in the negative regulation of tumorigenesis. Here, we found that DDR signaling poises a series of epigenetic events, resulting in activation of pro-tumorigenic genes but can go as far as reactivation of the pluripotency gene OCT4. Loss of DNA methylation appears to be a key initiating event in DDR-dependent OCT4 locus reactivation although full reactivation required the presence of a driving oncogene, such as Myc and macroH2A downregulation. Using genetic-lineage-tracing experiments and an *in situ* labeling approach, we show that DDR-induced epigenetic reactivation of OCT4 regulates the resistance to chemotherapy and contributes to tumor relapse both in mouse and primary human cancers. In turn, deletion of OCT4 reverses chemoresistance and delays the relapse. Here, we uncovered an unexpected tumor-promoting role of DDR in cancer cell reprogramming, providing novel therapeutic entry points for cancer intervention strategies.

INTRODUCTION

It is becoming increasingly evident that many, if not all, tumor types contain a subset of cells that are labeled positive for markers of DNA damage response (DDR) (Bartkova et al., 2006; Halazonetis et al., 2008). The DNA damage-induced ataxia telangiectasia mutated (ATM)/ataxia telangiectasia and Rad3-related (ATR) pathways have been implicated in negative regulation of cell cycle progression, induction of differentiation, as well as in the activation of apoptosis (Stracker et al., 2013). Further evidence from cancer-prone mouse models supports the role of these pathways in delaying the onset of cancer and reducing tumor burden (Bulavin et al., 2004; Reddy et al., 2010; Shreeram et al., 2006b). In turn, inhibition of these pathways in various mouse models leads to increased tumor size and invasiveness. In humans, activation of DDR represents an important early step in the suppression of tumorigenesis (Bartkova et al., 2006; Halazonetis et al., 2008). These observations laid grounds to suggest, which was subsequently experimentally proven, that DNA damage pathways might serve as a barrier to cancer progression (Reddy et al., 2010; Santos et al., 2014; Shreeram et al., 2006b). Undoubtedly, the immediate consequences of activating the DNA damage pathways are induction of apoptosis or/and senescence and protection from cancer. Under certain conditions, however, these protective mechanisms may not be fully operational. For example, hypoxia, which is normally present in a tumor tissue, may severely blunt the response to irradiation, protecting cancer cells and contributing to cancer spreading (Das et al., 2008; Harada et al., 2012). In this scenario, the DNA damage response, instead of eliminating cancer cells, may have other consequences.

It is well documented that gaps in radiation therapy worsen the outcome of patients suffering from epithelial cancers of the head and neck region and of the breast (Bese et al., 2005; Withers et al., 1988). The mechanisms of this phenomenon are incompletely understood but are generally attributed to increased cancer growth during treatment gaps. Cancer patients who have received chemotherapy often relapse, and most go on to develop more advanced diseases following their initial therapy. In addition, the role of low-dose irradiation in cancer initiation is well documented (Lagadec and Pajonk, 2012). DNA damage, via an increased mutation rate, is believed to either activate oncogenes or disable tumor suppressors, thus favoring tumorigenesis. However, low-dose chemotherapy or radiotherapy may also exert immediate tumor-promoting effects in large populations of cancer cells *in vitro*—an effect that cannot be explained by changes in mutation rates (Hu et al., 2012).

Recent clinical and pre-clinical data support the view that some cancers are organized hierarchically, with a small number of cells, including cancer stem cells (CSCs), that are functionally linked to continued malignant growth and contribute to cancer metastasis, recurrence, and drug resistance (Magee et al., 2012). The origin of these highly malignant cells, however, remains controversial (Visvader and Lindeman, 2012). The discovery of Yamanaka factors capable of reprogramming differentiated cells back into an embryonic stem cell (ESC)-like state, and the identification of a stem-cell-like or "self-renewal" gene expression signature that is predictive of patient outcome, lends credence to the role of
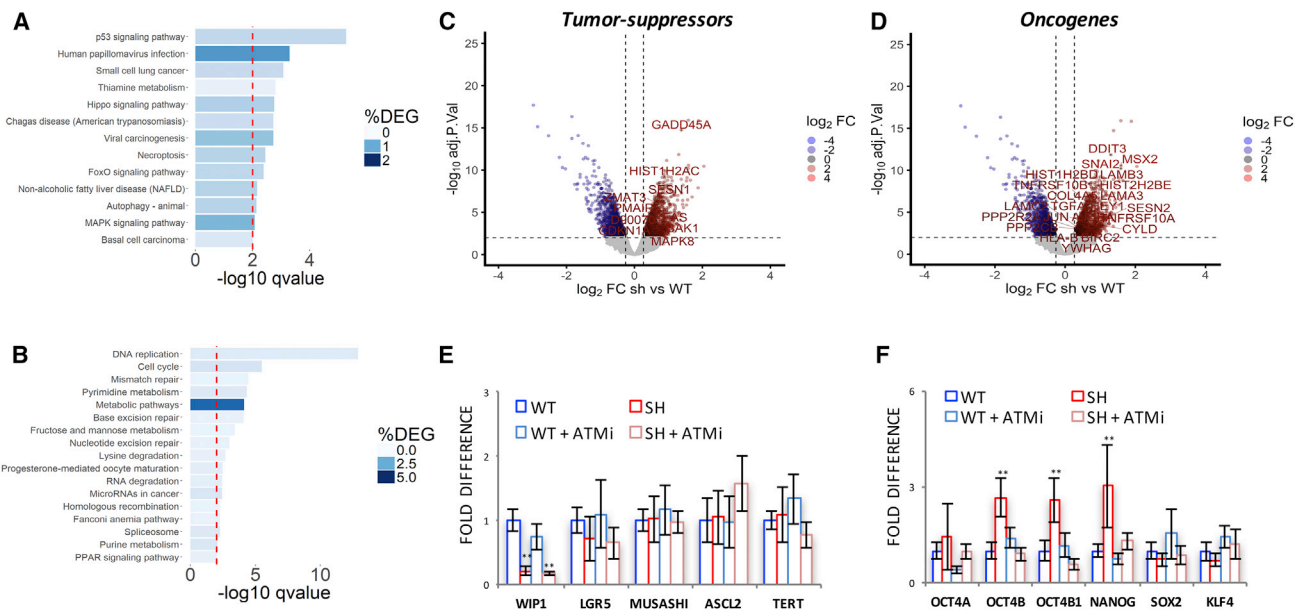
CellPress

Figure 1. Wip1 Regulates a Set of Tumor-Promoting Genes

Over-representation analyses for Kyoto Encyclopedia of Genes and Genomes (KEGG) pathways of differentially expressed genes in HCT116 WIP1 depleted (SH) versus WIP1 deficient treated with an ATM inhibitor KU55933 (AT_SH) and isogenic HCT116 cells (WT) at 5% false discovery rate (FDR).

(A and B) Upregulated (A) and downregulated (B) pathways with an over-representation FDR of 1% are shown.

(C) Volcano plot showing the most differentially expressed tumor suppressor genes in HCT116 WIP1-depleted versus isogenic HCT116 cells.

(D) Volcano plot showing the most differentially expressed oncogenes in HCT116 WIP1 depleted versus isogenic HCT116 cells.

(E) qRT-PCR analysis of adult stem cell markers in WIP1sh HCT116 cells with and without ATM inhibitor (SH + ATMi) relative to HCT116 WT (n = 3 biological replicates).

(F) qRT-PCR analysis of pluripotency genes in treatment conditions as indicated (n = 3 biological replicates). **p < 0.01.

Two-tailed paired (E and F) Student's t test. Data are mean ± SD.

early pluripotent genes and their clinical relevance (Eppert et al., 2011; Gentles et al., 2010; Takahashi and Yamanaka, 2006). OCT4 and NANOG expression predicts aggressive tumor behavior and worse clinical outcome in several types of cancer (Gwak et al., 2017; Murakami et al., 2015). Forced expression of these genes increases tumorigenesis, and depletion lowers tumorigenic potential (Hochedlinger et al., 2005; Kumar et al., 2012). The mechanism controlling the expression of pluripotency genes in cancer, however, remains largely unknown.

RESULTS

WIP1-Dependent DDR Signaling Controls Both Positive and Negative Regulators of Tumorigenesis

We have previously found that loss of the WIP1 phosphatase results in activation of the DNA damage response through modulation of the DDR signaling pathway; this activation occurs in the absence of physically damaged DNA and via upregulation of the activity of sensors of DNA damage, such as ATM (Shreeram et al., 2006a). Therefore, genetic models of WIP1 deletion or knockdown may faithfully replicate the conditions of enhanced DNA damage signaling (DDR) response and may provide novel insights into our understanding of certain aspects of epigenetic regulation during tumorigenesis.

To investigate further the potential role of DDR signaling in tumor progression, we performed microarray analyses in wild-type

and WIP1-depleted HCT116 cells (Figures 1A, 1B, S1A, and S1B). Gene set enrichment analysis showed the activation of several tumor-suppressor pathways in WIP1-depleted HCT116 cells (Figures 1A, 1C, and S1C). Surprisingly, we also observed an upregulation of several genes that represented different oncogenic and cancer-promoting pathways (Figures 1D and S1C). Both groups of genes were regulated in an ATM-dependent manner, as inclusion of a chemical inhibitor of ATM reversed the gene activation in WIP1-depleted cells (Figures S1A–S1C).

For further analysis, we focused on the mechanisms that may drive late stages of tumorigenesis. Specifically, tumor relapse has been associated with the formation of a subset of cells with unique properties, including the generation of CSCs. To better understand the impact of WIP1 knockdown, we examined whether CSC marker levels were changed upon WIP1 manipulation in colorectal cancer cells. However, our analysis revealed no change in the expression of the intestinal stem cell markers LGR5, TERT, MUSASHI, and ASCL2 (Figure 1E). In turn, several key transcription factors that are critical in ESC maintenance were also enriched in CSCs, including OCT4A and NANOG (Gwak et al., 2017; Murakami et al., 2015). We designed a panel of specific primers to separately examine the different OCT4 isoforms: OCT4A; OCT4B; and OCT4B1, but not a pseudogene. We found that WIP1-depleted HCT116 cells showed ATM-dependent enrichment of NANOG, OCT4B, and OCT4B1, but

not OCT4A (Figure 1F). This prompted us to speculate that, although WIP1 deficiency is not sufficient to reactivate the master regulator of pluripotency OCT4A, DDR signaling clearly has an impact on the genomic locus.

DNA Damage-Induced Signaling Controls DNA Methylation and Epigenetic Status of OCT4 Locus

Our analysis revealed that WIP1-depleted HCT116 cells showed ATM-dependent upregulation of the OCT4 isoforms OCT4B and OCT4B1 that are transcribed from a putative promoter located in the first intron (Livyatan et al., 2015). In turn, this suggested that, although the OCT4 gene is normally silenced by DNA methylation in somatic cells, the region of the first intron could be demethylated upon WIP1 depletion and ATM activation. To verify this, we analyzed DNA methylation using a DNA methylation immunoprecipitation (MeDIP) assay (Figure 2A). We found that the first intron was significantly demethylated in WIP1-depleted cells (Figure 2A, region Q), prompting us to investigate the impact of DDR signaling activation on OCT4 locus. Next, we extended our analysis to a 3-kb nucleotide sequence upstream of the OCT4 transcription start site (TSS) (Figure 2B) and to the promoters of the NANOG and SOX2 genes (Figures S2A and S2B). We did not find CpG islands in the 5′ end of the OCT4 gene, although CpG nucleotides were fairly abundant (Figure S2C). Gene walking across this 3-kb region showed extensive demethylation of the locus in WIP1-depleted cells (Figure 2B). In addition to the first intron, the erasure of DNA methylation occurred upstream of a distal promoter and in a distal enhancer (Figure 2B). All of these regions have been identified as functionally important regulatory elements of the OCT4 locus (Nordhoff et al., 2001). Similar to the OCT4 gene, the NANOG promoter showed demethylation in WIP1-depleted HCT116 cells (Figure S2A), and the SOX2 promoter was unaffected (Figure S2B). We confirmed the results of our DNA methylation analysis using another cancer cell line MCF7 (Figure S2D), with the use of a different antibody (Figure S2E), and after treatment with a WIP1 inhibitor (Figure S2F).

Next, we examined whether an ATM-dependent signaling pathway was responsible for changes in DNA methylation on the OCT4 locus. We performed 5meC immunoprecipitation experiments in the presence of a chemical inhibitor of ATM, which revealed that ATM signaling activation was required for demethylation of the OCT4 locus in WIP1-depleted HCT116 cells upstream of a distal promoter (region G), in a distal enhancer (region B), and in the first intron (Figure 2C, region Q). Further analysis showed that, upon WIP1 depletion, the reduction in DNA methylation on OCT4 regulatory elements correlated with DNMT3B displacement (Figure 2D). In contrast, we did not observe any WIP1-dependent regulation of DNMT1 binding on the OCT4 gene (Figures S2G and S2H). Importantly, DNMT3B overexpression was sufficient to increase DNA methylation of the OCT4 locus in HCT116 cells (Figure S2I).

We previously found that ATM activation leads to DNMT3B enrichment on heterochromatin-associated sequences, such as L1LINE (Filipponi et al., 2013). Considering the abundant nature of heterochromatin in a cell, DNMT3B displacement from the OCT4 sequences could result from its redistribution to heterochromatin. In this scenario, the dynamic of DNMT3B on the OCT4 locus would be dependent on BRCA1, as was previously shown for L1LINE sequences (Filipponi et al., 2013). Chromatin immunoprecipitation experiments showed that, in WIP-depleted cells, BRCA1 is displaced from the promoter and a distal enhancer (Figure S2J). Consistent with this prediction, we found that, in WIP1-depleted HCT116 cells, DNMT3B occupancy upstream of a distal promoter, on a distal enhancer, and in the first intron of the OCT4 gene was fully dependent on BRCA1 (Figures S2K and S2L). Correspondingly, depletion of BRCA1 restored DNA methylation on the OCT4 locus in WIP1-depleted HCT116 cells (Figure S2M).

Next, we checked whether activation of DDR signaling by other means than WIP1 depletion could impact the level of DNA methylation on OCT4 locus. As efficient DNA demethylation requires several rounds of DNA replication, first we established conditions for extended treatment of cells with a chemotherapeutic drug(s) without inducing a cell death or a permanent cell cycle arrest. Consistent with previous observations (Harada et al., 2012), we found that, in low oxygen conditions, a treatment of HCT116 cells for 12 days with cyclophosphamide induced sustainable activation of DDR signaling without causing apoptosis or cell cycle arrest (Figure 2E). Next, we analyzed the level of DNA methylation and found that cyclophosphamide strongly impacted the level of DNA methylation on OCT4 regulatory elements in an ATM-dependent manner (Figure 2F). Thus, similar to WIP1 depletion, a chemotherapeutic treatment regulates DNA methylation on OCT4 locus.

MacroH2A Counterbalances DNA Demethylation in Regulation of the OCT4 Locus

Previous findings revealed strong correlations between H3K9me2/3 methylation, DNA methylation, and gene silencing. We therefore determined the enrichment of H3K9me2/3 on the OCT4 locus. Chromatin immunoprecipitation (qChIP) assay results indicated that WIP1 depletion led to a marked decrease in the repressive histone mark H3K9me2/3 on both OCT4 (Figure 3A) and NANOG (Figure S3A) regulatory elements, correlating with reduced 5meC levels on these genomic sequences (Figures 2B and S2A). Next, we investigated whether the decrease of H3K9me2/3 was accompanied by a simultaneous increase of acetylation of lysine K9 that is associated with permissive chromatin for gene activation. We observed a negative correlation between methylation and acetylation of lysine 9 of histone H3 in both OCT4 (Figures 3A and 3B) and NANOG regulatory regions (Figure S3A). The H4 acetylation level and in particular H4K16Ac was also significantly enhanced in WIP1-depleted HCT116 cells (Figures 3C and S3B) and total histone occupancy was unchanged (Figure S3C). Next, we analyzed potential epigenetic modifiers that could modulate the level of acetylation. We found that histone deacetylase, SIRT1, is enriched on OCT4 regulatory regions and displaced in Wip1-depleted cells (Figure 3D). Although the displacement was partial, this still was sufficient to induce H3K9 and H4K16 acetylation (Figures 3B and 3D). These activating epigenetic modifications are critical for gene expression, and next, we asked whether activation of the remaining pool of SIRT1 on OCT4 would be sufficient to reduce these
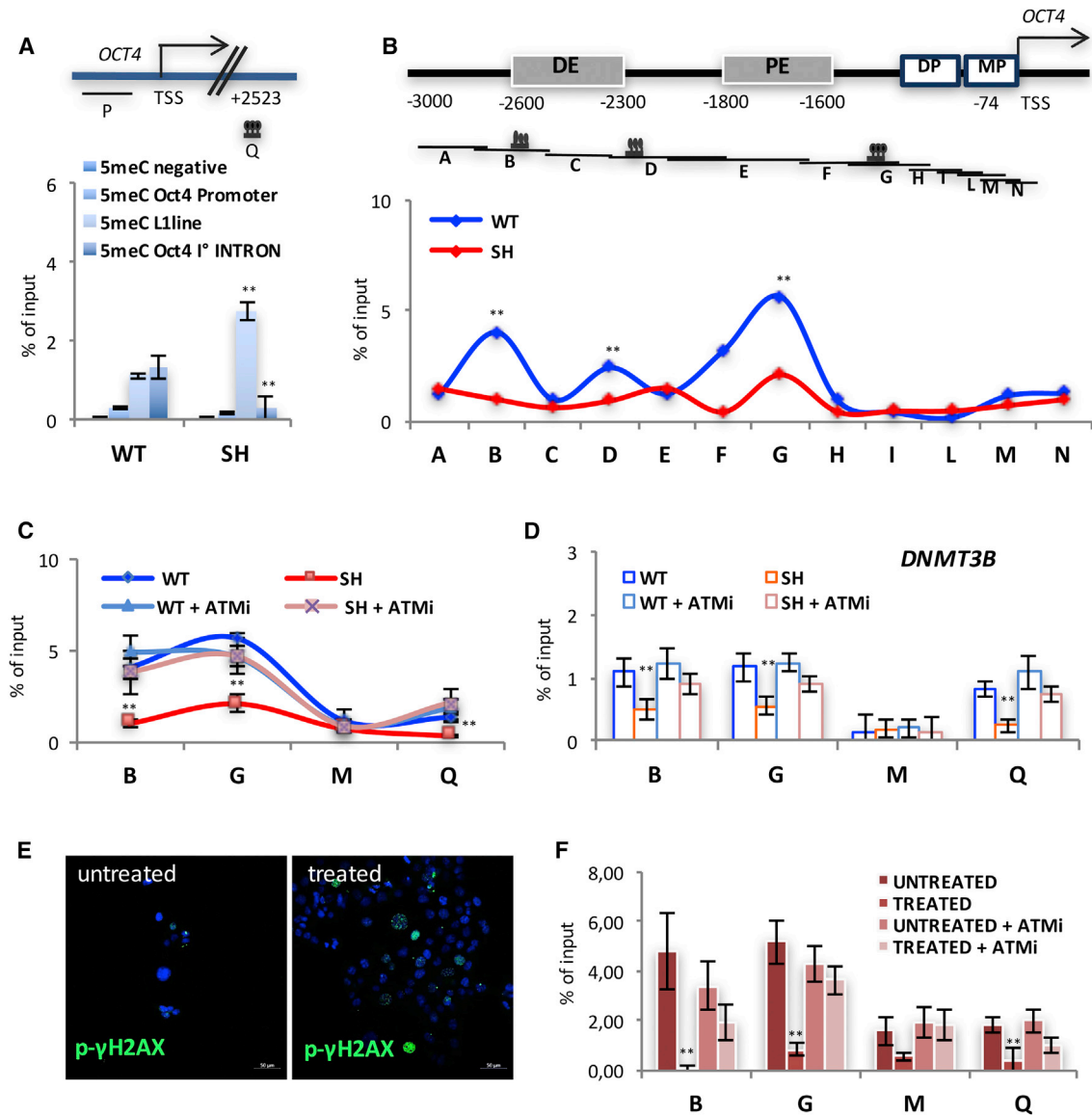
CellPress

Figure 2. DNA Damage-Induced Signaling Controls DNA Methylation and Epigenetic Status of OCT4 Locus

(A) (Top) Schematic representation of the first intron of the human OCT4 gene (GenBank: AJ297527). (Bottom) Analysis of 5meC enrichment in HCT116 SH (SH) and HCT116 WT is shown. Q, first intron regions; P, promoter regions; negative, control hUBE2B.

(B) (Top) Schematic representation of 3-Kb nucleotide sequence containing CpG sites upstream to OCT4 TSS. A–N designates the primer-amplified regions. DE, distal enhancer; DP, distal promoter; MP, minimal promoter; PE, proximal enhancer. (Bottom) DNA methylation pattern of OCT4 locus in parental (WT) and Wip1-depleted HCT116 cells (SH) is shown.

(C) Analysis of 5meC enrichment in HCT116 WT and WIP1SH with or without an ATM inhibitor KU55933 (ATMi). B, G, M, and Q, primer positions as shown in (A) and (B).

(D) ChIP analysis of DNMT3B occupancy in parental (WT) and Wip1-depleted (SH) HCT116 cells with or without an ATM inhibitor (ATMi).

(E) Confocal images of HCT116 cells treated with 10-μM cyclophosphamide for 12 days in 5% oxygen and stained with phospho- γH2AX antibody (green). DNA was counterstained with DAPI (blue).

(F) Analysis of 5meC enrichment in untreated and cyclophosphamide-treated HCT116 cells (as in E) with or without an ATM inhibitor KU55933.

**p < 0.01. Two-tailed paired Student's t test; data are mean ± SD.

marks. Consistently, treatment of HCT116 WIP1-depleted cells with a sirtuin activator, resveratrol, reversed the pattern of histone acetylation (Figure 3C), further supporting the idea that WIP1 depletion epigenetically poises the OCT4 locus for transcriptional activation. Despite these alterations, OCT4A mRNA levels re-

mained unchanged in WIP1-depleted cells (Figure 1F), indicating that both DNA demethylation and histone acetylation are insufficient for OCT4 gene reactivation. This suggested the existence of additional mechanisms responsible for silencing OCT4A transcription in WIP1-depleted cells.
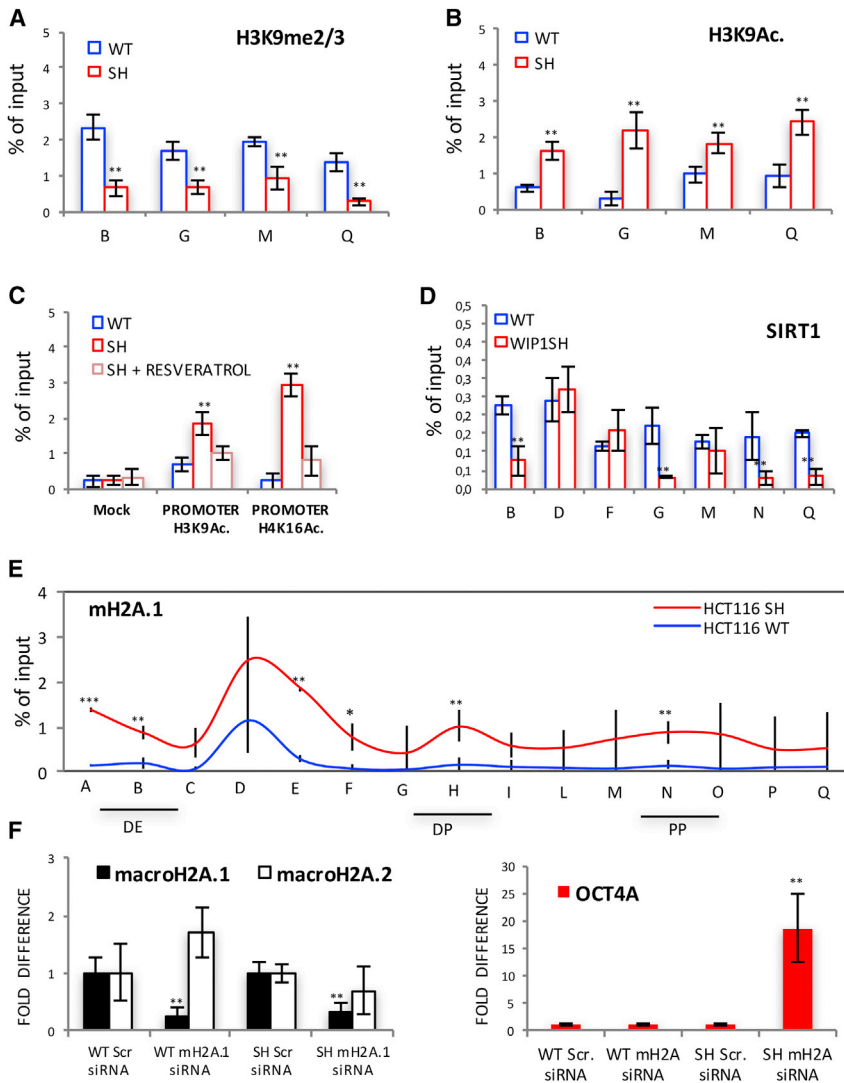
Figure 3. MacroH2A.1 Constrains OCT4A Reactivation in WIP1-Depleted Cells

(A and B) ChIP assay for H3K9me2/3 (A) and H3K9Ac (B) in parental (WT) and Wip1-depleted (SH) HCT116 cells.

(C) ChIP assay for enrichment of H3K9Ac and H4K16Ac in parental (WT) and Wip1-depleted (SH) HCT116 cells with or without resveratrol treatment.

(D) ChIP analysis of SIRT1 occupancy in parental (WT) and Wip1-depleted (SH) HCT116 cells.

(E) ChIP assay of macroH2A.1 occupancy on OCT4 locus in parental (WT) and Wip1-depleted (SH) HCT116 cells. A–N, primers position as in Figure 2B. PP, proximal promoter.

(F) qRT-PCR analysis of mH2A.1, mH2A.2, and OCT4A in HCT116 WT and WIP1 SH cells after macroH2A siRNA knockdown (mH2A.1siRNA) relative to HCT116 WT and SH Scrambled cells.

*p < 0.05; **p < 0.01; ***p < 0.001. Two-tailed paired Student's t test. Data are mean ± SD.

To test whether macroH2A occupancy on OCT4 regulatory elements restricted the transcriptional activation of OCT4A, we next knocked down macroH2A.1 in parental and WIP1-depleted HCT116 cells using the small interfering RNA (siRNA) approach (Figure 3F). Depletion of macroH2A.1 did not impact OCT4 expression in parental HCT116 cells (Figure 3F), which was consistent with the low background occupancy of mH2A.1 on the OCT4 locus (Figure 3E). In contrast, macroH2A.1 siRNA significantly enhanced OCT4 mRNA levels in WIP1-depleted HCT116 cells (Figure 3F). Thus, our data indicated that macroH2A could function as a transcriptional repressor, as its removal resulted in a 15- to 20-fold upregulation of OCT4A mRNA in WIP1-depleted HCT116 cells (Figure 3F). As OCT4A levels are extremely low in somatic cells, the observed OCT4A upregulation after macroH2A depletion remained far below the levels present in ESCs. Thus, we speculated that there should be further mechanisms that could positively contribute to activation of OCT4A.

MYC Cooperates with MacroH2A Knockdown in Transcriptional Regulation of the OCT4 Locus

In ESCs, OCT4A expression is regulated in a positive feedback manner by OCT4A itself. As somatic cells lack OCT4A, we focused on other transcriptional factors that could potentially drive OCT4A expression. Bioinformatics analysis of the OCT4 promoter sequence revealed the presence of several transcriptional binding sites for OCT4A as well as SOX2 and MYC. Next, we investigated whether overexpression of any of these factors would be sufficient to drive OCT4A expression. We found that none of the analyzed factors was sufficient to modulate OCT4A levels in parental HCT116 cells (Figure 4A), consistent

To investigate the potential mechanism(s) responsible for the lack of OCT4A transcriptional activation in WIP1-depleted cells, we performed a ChIP assay to examine epigenetic regulators that could suppress OCT4 reactivation in WIP1-depleted cells. We focused on epigenetic modulators that have been previously implicated in the regulation of pluripotency genes in ESCs, including SIRT1, SIRT6, KAP1, macroH2A, HDAC1, H2A.Z, H1.2, CTCF, G9A, p300, SUV39H1, EZH2, KDM3A, and AID (not shown). Among these tested genes, we found that macroH2A.1 was enriched on OCT4 gene in a WIP1-dependent manner. Next, we profiled the macroH2A.1 occupancy on the entire OCT4 locus (Figure 3E). Analysis of the OCT4 locus revealed low occupancy of macroH2A in parental HCT116 cells. In contrast, WIP1-depleted HCT116 cells showed significant enrichment of macroH2A.1 on the OCT4 gene (Figure 3E). Interestingly, macroH2A.1 occupancy was ATM, SIRT1, DNMT3B, and BRCA1 dependent (Figures S3D and S3E), further confirming the role of DDR signaling in regulation of OCT4 locus.
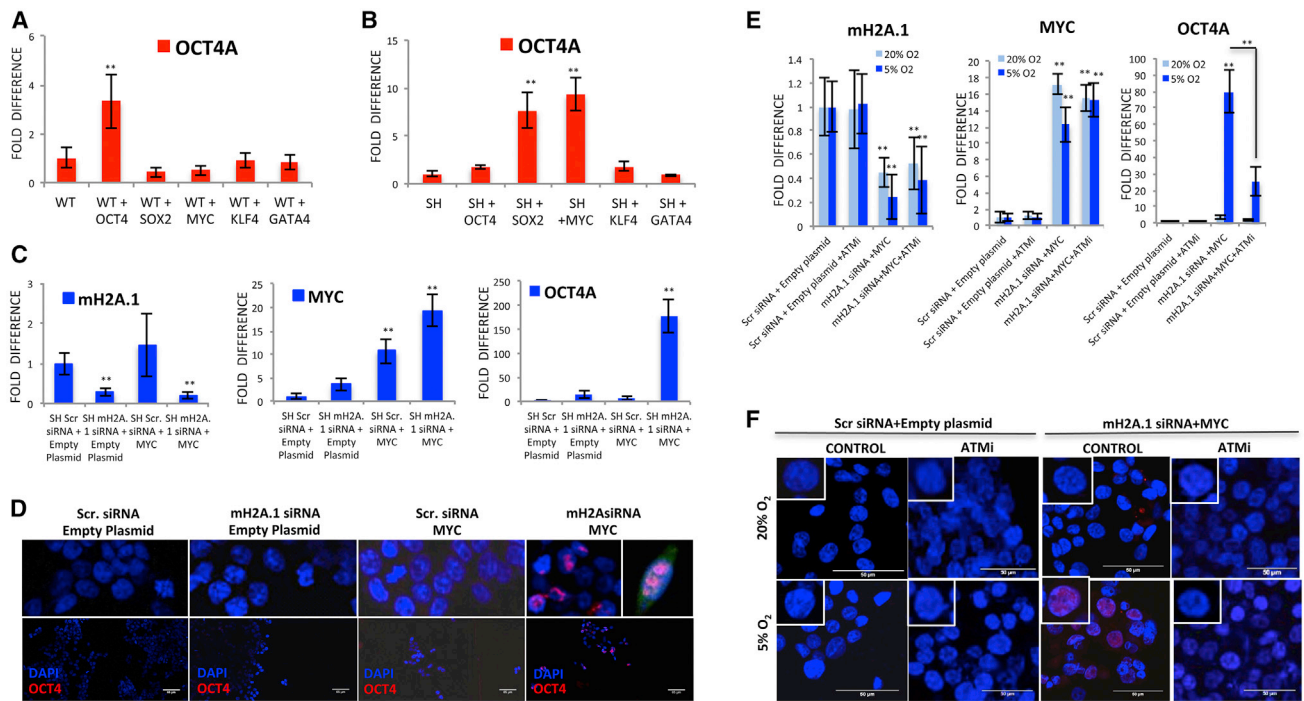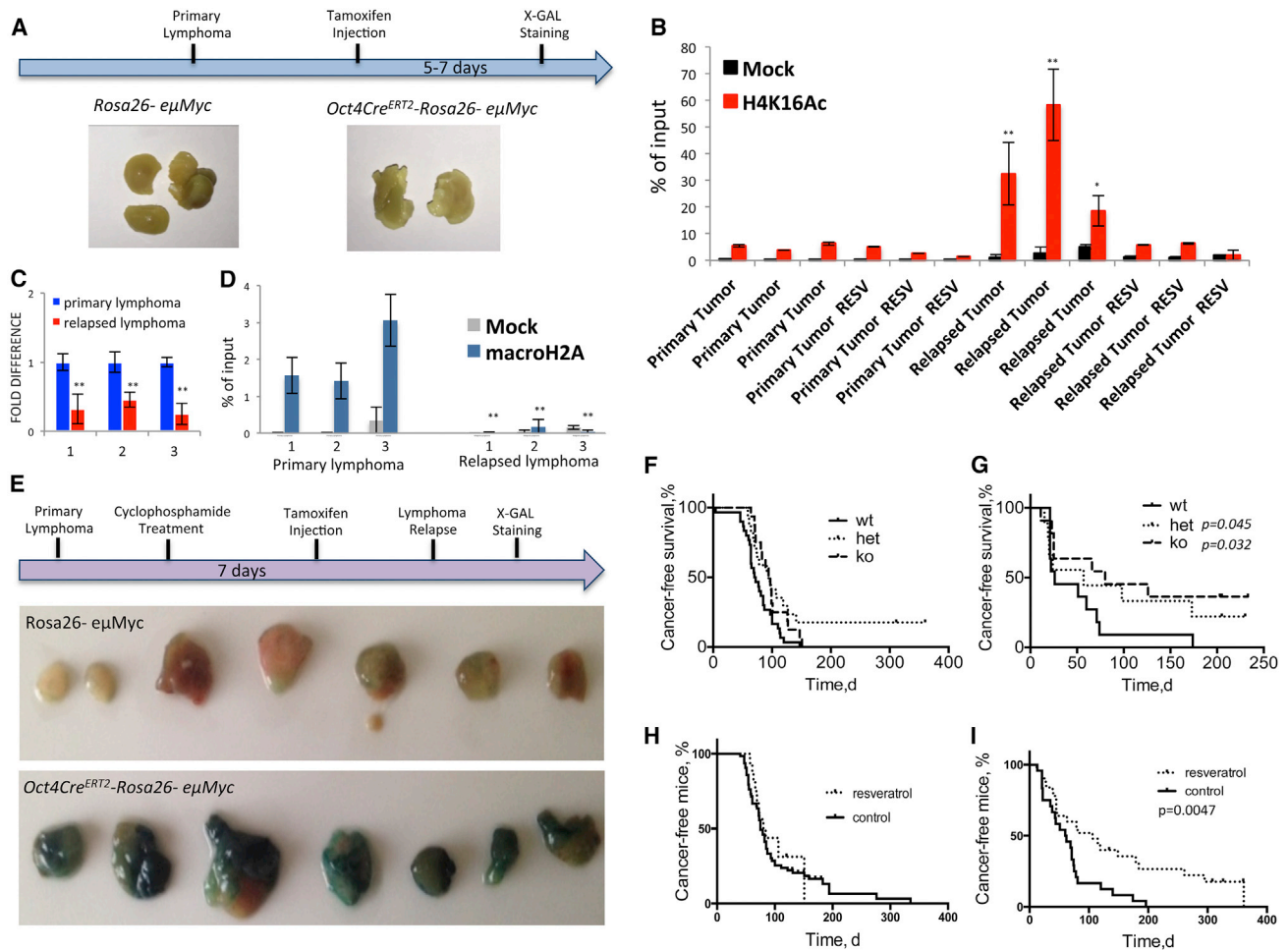
Figure 4. MYC Cooperates with macroH2A Knockdown in Transcriptional Regulation of OCT4 Locus
(A) qRT-PCR of OCT4A in parental HCT116 cells after OCT4A, SOX2, MYC, KLF4, and GATA4 overexpression.
(B) qRT-PCR of OCT4A in WIP1-depleted HCT116 cells (SH) after OCT4, SOX2, MYC, KLF4, and GATA4 overexpression.
(C) qRT-PCR of mRNA levels for macroH2A.1, MYC, and OCT4A in WIP1-depleted HCT116 cells (SH) after mH2A.1 siRNA, Myc overexpression, or both relative to Scr siRNA-treated cells.
(D) Confocal images of WIP1-depleted HCT116 cells stained for OCT4A after different treatments as indicated. DNA was counterstained with DAPI (blue).
(E) qRT-PCR of mRNA levels for macroH2A.1, MYC, and OCT4A in HCT116 cells treated with cyclophosphamide and cultured in 20% and 5% oxygen after mH2A.1 knockdown and MYC overexpression relative to Scr siRNA-treated cells.
(F) Confocal images of OCT4A staining of HCT116 cells treated with cyclophosphamide and cultured in 5% and 20% oxygen with and without ATM inhibitor after mH2A.1 knockdown and MYC overexpression. DNA was counterstained with DAPI (blue).
**p < 0.01. Two-tailed paired Student's t test. Data are mean ± SD.

with the fact that the locus is methylated and transcriptionally silent. However, in WIP1-depleted HCT116 cells, we found that overexpression of both MYC and SOX2, but not of OCT4A, GATA4, or KLF4, was sufficient to induce 10-fold upregulation of OCT4A mRNA levels (Figure 4B). In addition, both SOX2 and MYC overexpression induced the expression of NANOG mRNA, and SOX2 remained unchanged (Figure S4A). Our data suggest that alternative transcription factors, such as MYC and SOX2, may drive OCT4A expression when the locus is demethylated as in WIP1-depleted cells. This raised the possibility that simultaneous MYC upregulation and macroH2A downregulation could result in further reactivation of OCT4A transcription in WIP1-depleted HCT116 cells. We were particularly interested in this cooperative event because both MYC activation or overexpression and macroH2A downregulation are commonly present in advanced human cancers. To investigate this possibility, we knocked down macroH2A.1 and simultaneously overexpressed MYC in WIP1-depleted HCT116 cells (Figure 4C). We found a significant cooperative effect between these two events, resulting in a multiple fold increase of the OCT4A mRNA level (Figure 4C). Using immunofluorescent analysis, we re-confirmed the induction and nuclear accumulation of OCT4A protein after

macroH2A.1 knockdown and MYC overexpression (Figures 4D, S4B, and S4C). The simultaneous knockdown of macroH2A.1 and overexpression of MYC, in WIP1-depleted cells, also led to more robust activation of a NANOG locus, although SOX2 remained unaffected (Figure S4D). This transcriptional reactivation was abolished upon treatment with the phospho-POLII-Ser2/5 inhibitor flavopiridol (Figure S4E), suggesting that, in WIP1-depleted HCT116 cells, the OCT4 locus is reactivated thought a POLII-transcriptional-dependent mechanism.

Next, we asked whether the cooperative effect of MYC overexpression and macroH2A downregulation in activation of OCT4A transcription could occur when common chemotherapeutic drugs activate DDR signaling. For that, we treated HCT116 cells with cyclophosphamide and cultured them under different oxygen concentrations for 12 days. Analyses of OCT4A mRNA levels and OCT4A protein revealed their significant upregulation in cells cultured under low-oxygen conditions (Figures 4E and 4F). Importantly, these changes were significantly diminished in the presence of the inhibitor of ATM (Figures 4E and 4F). These data further support the role of DDR signaling in the regulation of OCT4A transcription.

Figure 5. Oct4A-Expressing Cancer Cells Contribute to Tumor Relapse

(A) (Top) Schematic representation of experimental design used to analyze Oct4 lineage tracing in primary eμ-Myc-driven B cell lymphomas. (Bottom) X-gal staining shows no Oct4 lineage tracing in primary tumors from Oct4Cre^{ERT2}-Rosa26-eμMyc and Rosa26-eμMyc mice.

(B) ChIP assay of H4K16Ac enrichment on Oct4 promoter in mouse primary lymphoma before cyclophosphamide treatment (1–3) and after relapse without (7–9) or with (3–6 and 10–12) resveratrol treatment. Analysis was carried out in 3 different tumors in triplicates.

(C) qRT-PCR analysis of mH2A.1 mRNA expression in relapsed lymphomas relative to primary tumors (tumors from 3 different mice).

(D) ChIP assay of macroH2A.1 enrichment on Oct4 promoter in mouse in primary lymphoma (1–3) and after relapse (4–6).

(E) (Top) Schematic representation of experimental design used to analyze Oct4 lineage tracing in relapsed tumors after cyclophosphamide treatment. (Bottom) X-gal staining shows a strong Oct4 lineage tracing in relapsed tumors from Oct4Cre^{ERT2}-Rosa26-eμMyc mice after cyclophosphamide treatment.

(F) Tumor-free survival (primary tumors) of Oct4 wt (wt) (n = 30), Oct4 conditional heterozygous (het) (n = 17), and Oct4 conditional knockout (ko) (n = 15) mice.

(G) Cancer-free survival of wt (n = 10), Oct4 conditional het (n = 9), and Oct4 conditional ko (n = 11) mice after cyclophosphamide treatment.

(H and I) Analysis of the onset of primary tumors (H) and tumor relapse (I) in eμ-Myc control mice or mice treated with resveratrol after cyclophosphamide treatment. Resveratrol was added to the drinking water at the age of 4 weeks, and mice were monitored for the onset of primary tumors. For relapse studies, resveratrol was added 7 days after cyclophosphamide injection to exclude the interference with chemotreatment.

*p < 0.05; **p < 0.01. Two-tailed paired Student's t test. Data are mean ± SD.

Oct4-Expressing Cancer Cells Contribute to Tumor Relapse

Our data showed that MYC overexpression could efficiently drive OCT4A transcriptional activation when the macroH2A level was reduced in cells with a demethylated OCT4 locus. MacroH2A downregulation is common in advanced cancers, and demethylation of the OCT4 locus can be imposed by DNA damage signaling, as we observed after WIP1 depletion or in the presence of a chemotherapeutic drug cyclophosphamide. To evaluate reactivation of the OCT4 locus *in vivo*, next, we per-

formed genetic-lineage-tracing experiments using a tamoxifen (TAM)-inducible mouse line in which Cre^{ERT2} was knocked into the Oct4 locus. We crossed these mice with a Rosa26-LacZ reporter line and subsequently with eμ-Myc transgenic mice, a non-CSC model of B cell lymphoma, in which any cancer cell can give rise to lymphoma in a transplantation assay (Kelly et al., 2007). Once tumors developed, we injected mice with TAM, and we sacrificed them 1 week later. We observed no lineage tracing in primary lymphomas, suggesting that reactivation of the Oct4 locus in primary tumors does not occur (Figure 5A).

Next, we investigated whether Oct4a-expressing cells appeared in response to cancer treatment and, if so, how they might contribute to tumor relapse. We used a single cyclophosphamide treatment on developed lymphomas and considered efficient remission to have occurred if no tumor was observed 1 week post-injection ("0" time point). On average, tumors relapsed in 5–10 weeks in eμ-Myc control mice. As SIRT1 plays an important role in establishment of the epigenetic status of OCT4 locus in response to activation of DNA damage signaling (Figures 3C and 3D), next, we turned to the analysis of histone acetylation in primary and relapsed eμ-Myc tumors. We found a significant increase in H4K16 acetylation within the Oct4 promoter in relapsed cancers compared to primary tumors. Importantly, this increase was reversed in mice treated with resveratrol (Figure 5B). Next, we analyzed the macroH2A.1 levels in relapsed versus primary tumors and found that relapsed eμ-Myc-driven B cell lymphomas showed decreased macroH2A.1 mRNA levels (Figure 5C). Furthermore, we found that macroH2A occupancy on Oct4 promoter was significantly reduced in relapsed versus primary B cell lymphoma in mice (Figure 5D). This observation encouraged us to further investigate the Oct4-dependent lineage tracing in relapsed tumors. To this end, two groups of mice (eμ-Myc/Oct4-Cre[ERT2]/Rosa26-LacZ and eμ-Myc/Rosa26-LacZ) were allowed to develop primary tumors and were subsequently treated with cyclophosphamide. When the tumors subsided 1 week later, the mice were injected with TAM and were observed for relapse. Upon tumor reappearance, the mice were sacrificed and lineage tracing was analyzed. Lineage tracing analysis revealed that the bulk of relapsed lymphomas were positive for X-gal staining, specifically in mice having the Oct4-Cre[ERT2] knockin, but not in control animals (Figure 5E). Of note, no lineage tracing was observed when TAM was injected either in the primary lymphoma before cyclophosphamide treatments or in a relapsed tumor (Figure S5).

To verify that Oct4 expression was critical for tumor relapse, we next turned to the analysis of Oct4 conditional knockouts. We crossed these mice with Rosa26-Cre[ERT2] and subsequently bred them with eμ-Myc transgenic mice. Further analyses were performed using three groups of mice: Oct4^{+/+}/Rosa26-Cre[ERT2]/eμ-Myc, Oct4^{+/−}/Rosa26-Cre[ERT2]/em-Myc, and Oct4^{−/−}/Rosa26-Cre[ERT2]/eμ-Myc were used for further analysis. We conditionally deleted Oct4 in 1-month-old mice by three consecutive daily injections of TAM. Oct4 deletion from adult somatic tissues did not result in any evident phenotype, suggesting that Oct4 is largely dispensable for postnatal tissue homeostasis (Lengner et al., 2007). Our analysis of primary lymphoma onset revealed no difference between groups, indicating that Oct4-expressing cells, if any, do not contribute to the primary tumor growth *in vivo* (Figure 5F). In sharp contrast, we found that tumor recurrence after cyclophosphamide treatment was significantly delayed in Oct4 heterozygous mice and even further delayed in Oct4-knockout mice (Figure 5G). Importantly, resveratrol significantly delayed the tumor relapse, but not the onset, of primary tumors in eμ-Myc transgenic mice (Figures 5H and 5I), further providing a link between epigenetic remodeling and a cancer treatment outcome.

OCT4 Methylation Serves as a Predictor of Cancer Patient Survival in Multiple Human Cancers

To investigate the predictive value of OCT4A mRNA expression, next, we turned to the analysis of patient survival in 32 human cancers available in The Cancer Genome Atlas (TCGA) datasets. The Andersen modified Peto-Peto survival estimate identified only one cancer type that showed a strong correlation between OCT4A mRNA levels and the patient survival, brain low-grade glioma (LGG) (Figure 6A). These results were not unexpected, as our model predicts that OCT4A could only be transiently induced and, as such, its levels are not necessarily increased in cancer. In contrast, the methylation status of OCT4 locus could be a stable epigenetic mark and, as such, could serve a better predictor of cancer patient survival. To verify that, first we determined the list of OCT4 methylation probes that show a strong negative correlation with OCT4A mRNA levels across all cancer samples found in TCGA dataset. We further mapped MYC-binding sites based on the results of more than 200 ChIP sequencing (ChIP-seq) data deposited in the University of California, Santa Cruz (UCSC) database (Figure 6B). Among 38 identified probes, 13 probes were present directly in the area of a MYC-binding site 1 (mbs1) located 10 kBp upstream of TSS. Other 4 probes were in the close vicinity of mbs2 and mbs3 located 5 kBp from TSS and in the first intron, respectively. Importantly, the methylation status of all three MYC-binding sites was reduced in WIP-1-depleted HCT116 cells in an ATM-dependent manner (Figure 6C). We further found that, in HCT116 cells, MYC binding on MBS3 is regulated in a WIP1-dependent manner (Figure 6D).

A Cox proportional hazards regression model was used to calculate the methylation levels (beta) as a predictor, and the hazard ratio was subsequently extracted. Multiple cancer types showed a strong correlation between OCT4 probe demethylation and poor prognosis (Figure 6E, left panel). We next turned to the analysis of a subset of patients with a top 50% of MYC mRNA expression levels. We observed an appearance of strong correlation for multiple probes located in mbs1 for esophageal cancer (TCGA-ESCA), lung squamous cell carcinoma (TCGA-LUAD), glioblastoma (TCGA-GBM), and rectum adenocarcinoma (TCGA-REAP) (Figure 6E, right panel). Of note, the level of MYC mRNA did not reach the significance as a predictor of patient survival in these 4 cancers (not shown). Thus, the epigenetic methylation status of OCT4 gene in several MYC-binding regions could serve as a potential prognostic marker of cancer patient survival across different tumor types.

OCT4A Expression Is Induced by DDR and Modulates the Response to Chemotherapy in Human Primary Tumors

Our proposed model implies the stochastic nature of the reprograming of cancer cells into cells that could potentially give rise to a tumor relapse. To provide direct evidence for OCT4A reactivation in human primary cancers in response to DDR, we next generated a genetic-lineage-tracing tool with CRISPR-Cas9 integration of CRE-ERt2 cassette into the endogenous OCT4 locus (Figures 7A and S6A–S6D) coupled with a TurboGreen reporter system. For this set of experiments, we focused on cancer types that do not show a significant demethylation of OCT4 locus to evaluate the full impact of DNA damage on locus
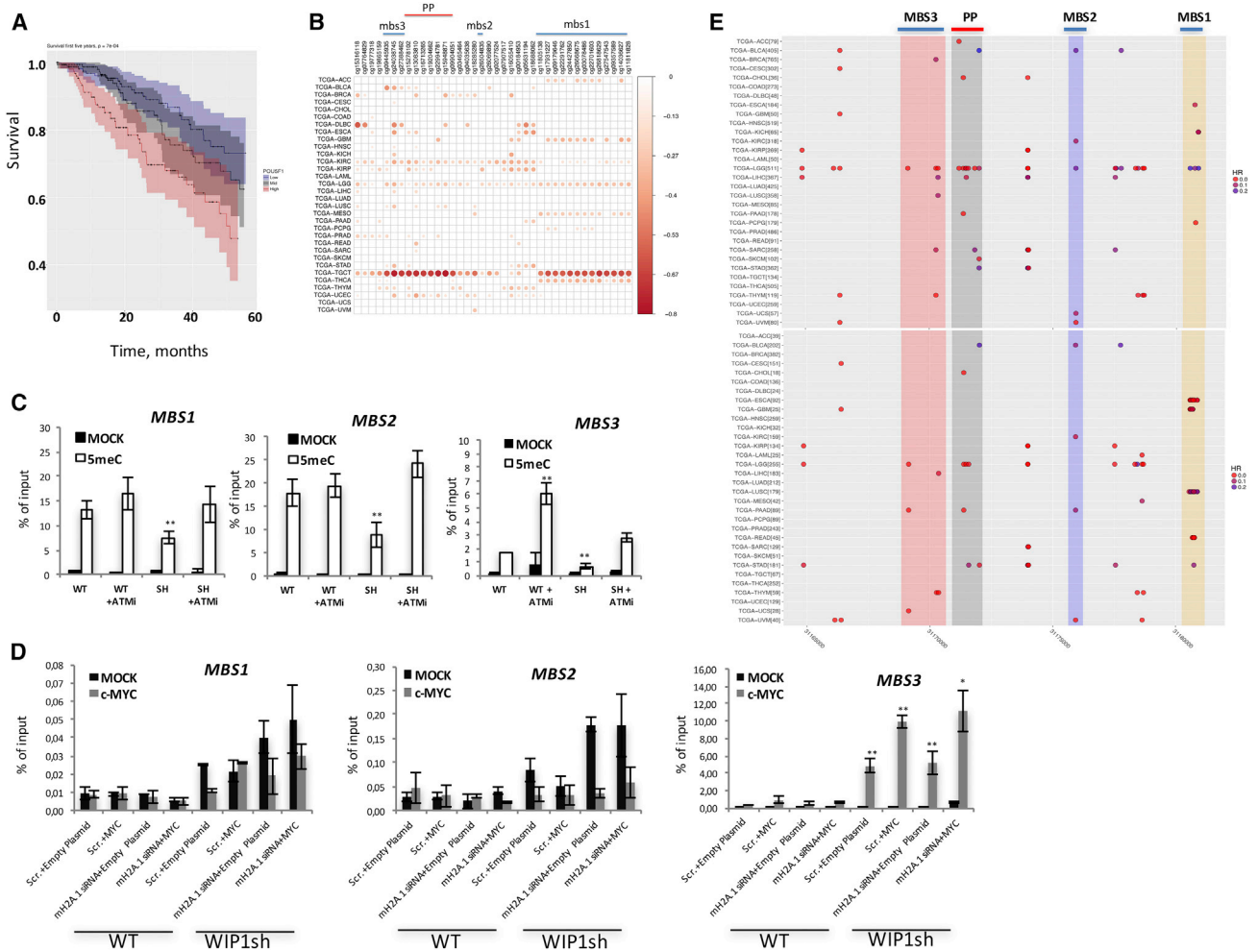
Figure 6. Analysis of Methylation Status of OCT4 Gene as a Predictor of Cancer Patients Survival

(A) Poor prognosis of lower grade glioma patients with high OCT4A (POU5F1) mRNA expression. Survival plot of 506 LGG patients from TCGA is shown. Patients were stratified into three groups according to OCT4A (POU5F1) mRNA expression levels, and Kaplan-Meier survival curves were calculated using the survfit command in R for the first 5 years of follow up. Trend p values were calculated using the Andersen modified Peto-Peto survival estimate.

(B) Expression levels of OCT4A (POU5F1) mRNA correlate broadly with methylation levels at the promoter and MYC-binding sites. All Illumina 450 methylation array probes mapped to hg38 and within the OCT4 gene, including 10-kBp promoter region, were downloaded from TCGA, and probes with less than 30 patients were removed from the analysis. Spearman rho of OCT4A mRNA expression to methylation levels was calculated for each probe, and only significant ($p < 0.05$) and negative correlations are displayed here for clarity.

(C) 5meC enrichment within the MYC-binding sites in WT and WIP1-depleted HCT116 cells with and without an ATM inhibitor KU55933. MBS1, MBS2, MBS3, MYC-binding sites as indicated in (B).

(D) ChIP assay of c-MYC occupancy on MYC-binding sites in HCT116 WT and WIP1-depleted cells after indicated treatments.

(E) Methylation levels in several regions of the OCT4 (POU5F1) gene, including 3 MYC-binding sites, are poor prognosis markers. All Illumina 450 methylation array probes mapped to hg38 and within the OCT4 gene were downloaded from TCGA, and probes with less than 30 patients were removed from the analysis. Cox proportional hazards regression model was calculated using the methylation levels (beta) as predictor. Hazard ratio was extracted and color coded. Only probes with log rank test significant ($p < 0.05$) probes and probes with hazard ratios below one are displayed in this figure for clarity: (left graph) all patients and (right graph) subset of patients within highest 50 percentile of MYC (uc003ysi) mRNA expression levels. Mbs stands for MYC-binding site.

*$p < 0.05$; **$p < 0.01$. Two-tailed paired Student's t test. Data are mean ± SD.

reactivation (Figure 6E). For that reason, primary cancer lines have been established from patients with lung adenocarcinoma (T27) and head and neck cancer (HN30). Correctly targeted T27 cells were injected into NOD scid gama (NSG) mice to grow tumors orthotopically in the lung, and 7 days later, one group of mice was treated with cisplatin and tamoxifen was injected next day. Our analysis of lineage tracing revealed the appear-

ance of progeny of OCT4-positive cells; this effect was significantly increased after the treatment with cisplatin (Figure 7B). Importantly, a stable depletion of ATM with short hairpin RNA (shRNA) efficiently reversed OCT4 reactivation after cisplatin treatment (Figure 7B).

Next, we investigated whether cells containing a DDR signature did in fact exhibit changes in the expression of pluripotency
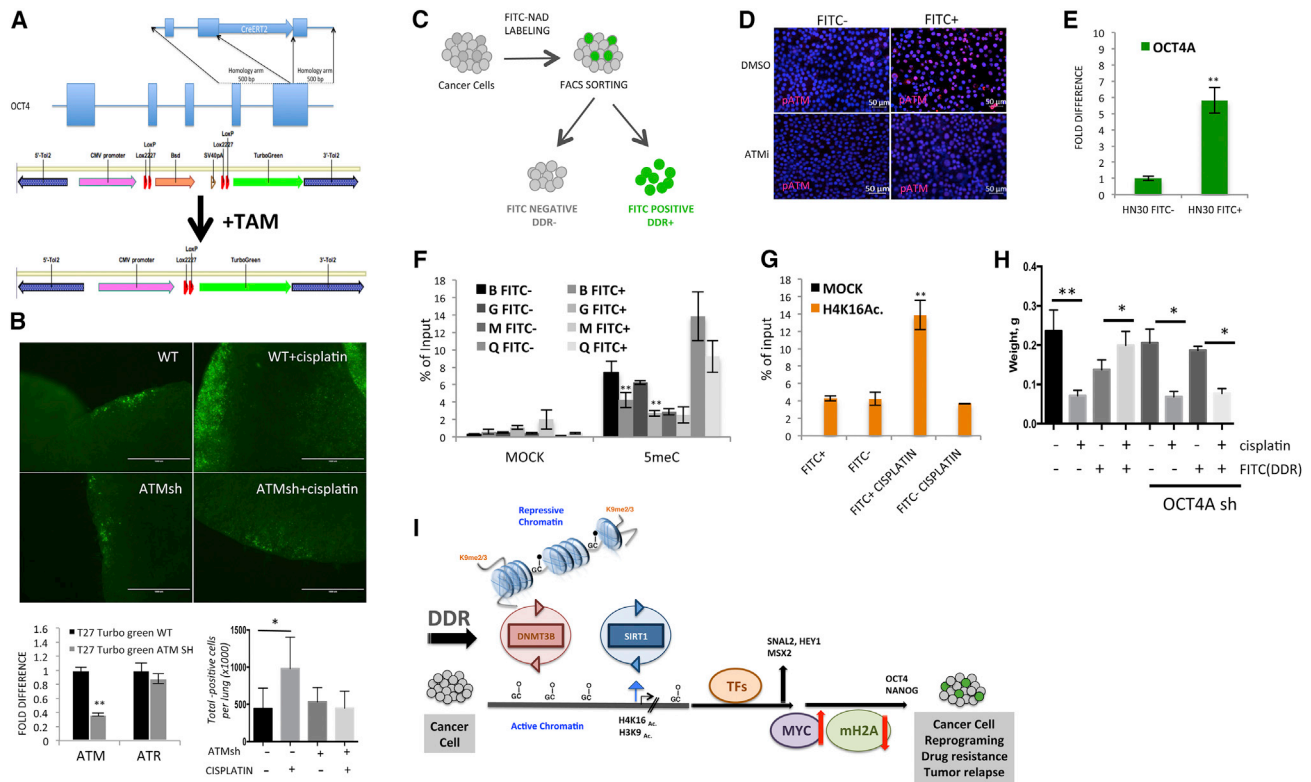
Figure 7. OCT4A Expression Is Induced by DDR and Modulates the Response to Chemotherapy in Primary Human Cancers

(A) Schematic representation of CRISPR/Cas9 targeting and lineage-tracing strategies used to analyze OCT4A lineage tracing in primary human cancer cells. Inclusion of TAM results in removal of a stop cassette and expression of TurboGreen in OCT4A-expressing cells and subsequently in their progeny.

(B) Genetic-lineage-tracing analysis of OCT4A-expressing cells in orthotopically (lung) parental and ATMsh grown primary human lung cancer cells. Analysis of ATM and ATR mRNA levels by RT-PCR was carried out in control and ATM shRNA cells (bottom left). The total number of TurboGreen-positive cells was calculated in the entire lung after full digestion (n = 5, bottom right).

(C) Schematic representation of FITC-labeling assay to enrich for DDR-positive cells.

(D) FITC+ and FITC− cells were purified from HN30 cells and stained for phospho-ATM after or without treatment with an ATM inhibitor (ATMi). DNA was counterstained with DAPI (blue).

(E) qRT-PCR shows the analysis of OCT4A mRNA levels in FITC+ cell fraction related to FITC− in primary patient-derived HN30 cells.

(F) 5meC enrichment in FITC+ and FITC− fractions purified from HN30 cells. B, G, M, and Q, primer positions as showed in Figure 2B.

(G) ChIP assay of H4K16Ac enrichment on OCT4 promoter in xeno-transplanted DDR-negative (FITC−) and DDR-positive (FITC+) HN30 cells. Some mice were treated with cisplatin 7 days after injection of cancer cells, and H4K16Ac enrichment was analyzed 2 weeks later.

(H) FITC-sorted DDR (+) and DDR (−) HN30 cells were injected into NSG mice and subsequently treated with cisplatin. In parallel, OCT4 was knocked down by shRNA, and FITC-positive and negative cells were injected and analyzed for sensitivity to cisplatin. The size of the tumors was measured 4 weeks later.

(I) A model for DNA damage-induced cancer cell reprogramming. For more details, see text.

*p < 0.05; **p < 0.01. Two-tailed paired Student's t test. Data are mean ± SD.

genes, including OCT4. We developed an assay to perform the in situ labeling of live cells that experienced DDR activation. Poly-ADP ribose polymerase (PARP) is robustly induced in response to DNA damage signaling activation, producing long chains of PAR conjugates. We used fluorescein isothiocyanate (FITC)-labeled nicotinamide adenine dinucleotide (NAD) as a PARP substrate to generate stable PAR-FITC conjugates in cells with active DDR (Figures 7C and S6E). First, we confirmed the specificity of the assay by showing that both PARP and ATM inhibitors strongly reduced the fraction of FITC-positive cells (Figure S6E). Next, we FITC labeled and sorted DDR/FITC-positive and DDR/FITC-negative cells and checked for the activation of DDR signaling. The DDR+ fraction showed a strong ATM- and PARP-dependent enrichment for a marker of DDR

signaling, phospho-ATM (Figures 7D and S6F). Of note, in DDR-positive cells, the enrichment for DDR markers was more robust than after depletion of HCT116 wild-type (WT) for WIP1 (Figure S6G). Next, we analyzed DDR/FITC-positive cells in a panel of human cancer cell lines and primary human cancers and found that they were enriched for OCT4A mRNA expression (Figures 7E and S6H), and the level of MYC and macroH2A.1 was similar between fractions (Figure S6I). Analysis of the epigenetics status of OCT4 locus in DDR/FITC-positive cells revealed significantly reduced levels of DNA methylation when compared to DDR-negative fractions in both patient-derived HN30 cells and HCT116 (Figures 7F and S6J). The DDR/FITC-positive fraction of HN30 cells shows increased levels of DDR signaling, and they were further amplified (3-fold

based on fluorescence-activated cell sorting [FACS] analysis) after cisplatin treatment (Figures S6K and S6L). Similar to HCT116 cells (Figures 4E and 4F), cisplatin treatment under low oxygen conditions cooperated with macroH2A.1 knock-down and MYC overexpression in an ATM-dependent OCT4A protein accumulation in HN30 cells (Figures S6M and S6N).

To understand the significance of OCT4A upregulation *in vivo*, we injected FITC-sorted DDR-positive and negative HN30 cells into NSG mice and treated them with cisplatin. H4K16 acetylation of OCT4 promoter was robustly induced and maintained after cisplatin treatment only in a DNA damage-positive fraction of xeno-transplanted primary human cancer cells (Figure 7G). We further found that cisplatin efficiently reduced the size of tumors from DDR-negative fraction (Figure 7H). In contrast, DDR-positive cells responded to cisplatin by further growth; this effect was fully eliminated by knocking down OCT4 with shRNA (Figure 7H).

DISCUSSION

The CSC model has been broadly accepted as an explanation for the clinical behavior of some cancers (Magee et al., 2012; Meacham and Morrison, 2013; Visvader and Lindeman, 2012). CSCs represent a distinct population of cells capable of clonal long-term repopulation and self-renewal, which can be prospectively isolated using different approaches. However, the observation that many cancers re-emerge after treatment does not necessarily imply that the cells that survive therapy are intrinsically more resistant than the cells that are killed. In a different scenario, a majority or even all of the cells within a given tumor might have a similar chance of surviving and expanding after therapy. This ability to survive could be directly linked to epigenetic changes that can be acquired during cancer treatment. In such a scenario, the lack of hierarchical organization within a tumor would support a model for clonal evolution of cancer (Nowell, 1976). In a recent report, Shaffer et al. (2017) argued that a transient epigenetic state could be responsible for acquisition of drug resistance in a subset of cancer cells. Here, we provide evidence that the DDR plays a key role in cancer cell reprogramming that can go as far as reactivation of the pluripotency gene OCT4 as summarized in Figure 7I. Our data indicate that a cancer cell that undergoes a series of epigenetic reprogramming events could have a similar chance of surviving and expanding after therapy.

Undoubtedly, the immediate consequence of DDR signaling activation—which can occur in response to cancer treatment or be typically present in a subset of primary cancer cells *in vivo*—is induction of apoptosis or/and senescence and thus protection from cancer. However, these mechanisms may not be fully operational under certain conditions. For example, hypoxia is normally present in tumor tissue and may severely blunt the response to irradiation, protecting cancer cells and contributing to cancer progression (Das et al., 2008; Harada et al., 2012). Our data suggest that, in cases where DDR signaling strength is insufficient to eliminate cancer cells, it can drastically change their transcriptional profiles to favor tumorigenesis and thus promote tumor relapse.

Here, we found that activation of DDR signaling was sufficient to remove DNA methylation at certain essential regulatory ele-

ments, including OCT4 and NANOG. Downstream of ATM activation, BRCA1 appeared to play a key role as a regulator of heterochromatin homeostasis, orchestrating the targeting of DNMT3B to heterochromatin-associated sequences (Figures S2J–S2M). Following DNMT3B displacement from defined genomic loci (including the promoter regions of OCT4 and NANOG), DNA methylation was lost. In fact, overexpression of DNMT3B in WIP1-depleted HCT116 cells re-established DNA methylation of essential regulatory regions of the OCT4 locus (Figure S2I). In addition to reduced DNA methylation, we observed increased histone acetylation at various regulatory elements, strongly supporting a role for DDR signaling in creating a favorable chromatin landscape for gene activation. However, although it seems necessary, DNA demethylation was insufficient to reactivate the major isoform OCT4A. This suggests that compensatory mechanisms may occur to silence critically important pluripotency genes when cells are challenged to undergo epigenetic reprogramming. Indeed, DDR signaling increased the occupancy of repressive markers, such as macroH2A.1, on OCT4 locus (Figure 3E). MacroH2A is globally deposited at silenced pluripotency genes, including Oct4, during developmental processes and ESC differentiation (Buschbeck et al., 2009). A recent large-scale screening revealed that macroH2A is associated with larger transcriptionally repressed regions, and synergy between DNA methylation and macroH2A deposition in the maintenance of a silenced state has been described (Creppe et al., 2012). Similarly, we observed a strong correlation between macroH2A occupancy and reduced levels of DNA methylation of the OCT4 locus following WIP1 depletion. Our data indicated that, within the context of a DDR response, macroH2A incorporation could act as a transcriptional barrier to constrain OCT4A reactivation once the locus becomes hypomethylated.

Recruitment of macroH2A efficiently counterbalances the role of the DDR response in OCT4A reactivation in cancer cells. However, advanced tumors exhibit significantly reduced macroH2A expression (Cantariño et al., 2013; Sporn et al., 2009). In such cases, an activated DDR response that is either continuously present in a distinct subpopulation of cancer cells or acutely induced by cancer treatment could result in epigenetic remodeling of the OCT4 locus into an active state. As demethylation occurs during rounds of DNA replication, in order to undergo demethylation in response to activated DDR signaling, cells must proliferate. In this respect, weak DDR signaling activators, such as after depletion of Wip1 or low doses of DNA damaging drugs, could be the most efficient inducers of cancer cell reprogramming. Although DDR-induced demethylation and macroH2A downregulation are necessary for OCT4 locus reactivation, they are not fully sufficient, and the additional involvement of various transcriptional drivers is critical. Here, we identified two transcriptional factors, MYC and SOX2, which are both overexpressed and activated in various human cancers. We showed that MYC overexpression together with macroH2A knockdown had an additive effect on enhancing reactivation of the OCT4 locus within the context of DDR activation (Figures 4 and S4). This transient reactivation of OCT4A could be a core factor contributing to cancer therapy failure. These OCT4A-expressing cancer cells efficiently contributed to tumor relapse

CellPress

both in the mouse and human cancers. In turn, depletion of OCT4 delays tumor relapse in mice (Figure 5) and restores chemosensitivity in human tumors (Figure 7). The reprogramming event described here mimics some properties ascribed to CSCs, yet without a cancer cell necessarily committing to a CSC model. In particular, we argue that drug resistance and the expression of pluripotency markers, which are considered as some features of CSCs, could also be attributed to the appearance of DDR-induced transient OCT4A-expressing cancer cells. Our work supports a model in which many, if not all, cancer cells independent of hierarchical organization can be challenged by DDR signaling to undergo epigenetic reprograming, including reactivation of OCT4A, thus contributing to tumor relapse.

STAR★METHODS

Detailed methods are provided in the online version of this paper and include the following:

- KEY RESOURCES TABLE
- CONTACT FOR REAGENT AND RESOURCE SHARING
- EXPERIMENTAL MODEL AND SUBJECT DETAILS
  - ○ Animal Experimentation
- METHOD DETAILS
  - ○ Cell Culture and treatments
  - ○ Labeling of live cells for activation of DNA damage signaling
  - ○ Immunofluorescence
  - ○ Chromatin Immunoprecipitation
  - ○ DNA Methylation Analysis
  - ○ Gene Expression and Microarray Analysis
  - ○ CRISPR/Cas9-mediated knock-in of CreERT2 into human OCT4 locus and genetic lineage tracing
  - ○ Bioinformatics analysis
  - ○ Statistical analysis
- DATA AND SOFTWARE ACCESSIBILITY

SUPPLEMENTAL INFORMATION

Supplemental Information can be found online at https://doi.org/10.1016/j.molcel.2019.03.002.

AUTHOR CONTRIBUTIONS

D.F. designed experiments, carried out most of the experiments, analyzed the data, and wrote initial draft; A.E. and J.M. designed and carried out some experiments; C.M. was responsible for the mouse colony and carried out some experiments; J.N. provided Oct4 conditional knockout mice; and D.V.B. secured funding, conceived the project, designed experiments, and wrote the manuscript.

DECLARATION OF INTERESTS

The authors declare no competing interests.

REFERENCES

Bartkova, J., Rezaei, N., Liontos, M., Karakaidos, P., Kletsas, D., Issaeva, N., Vassiliou, L.V., Kolettas, E., Niforou, K., Zoumpourlis, V.C., et al. (2006). Oncogene-induced senescence is part of the tumorigenesis barrier imposed by DNA damage checkpoints. Nature 444, 633–637.

Bese, N.S., Sut, P.A., and Ober, A. (2005). The effect of treatment interruptions in the postoperative irradiation of breast cancer. Oncology 69, 214–223.

Brichkina, A., Bertero, T., Loh, H.M., Nguyen, N.T., Emelyanov, A., Rigade, S., Ilie, M., Hofman, P., Gaggioli, C., and Bulavin, D.V. (2016). p38MAPK builds a hyaluronan cancer niche to drive lung tumorigenesis. Genes Dev. 30, 2623–2636.

Bulavin, D.V., Phillips, C., Nannenga, B., Timofeev, O., Donehower, L.A., Anderson, C.W., Appella, E., and Fornace, A.J., Jr. (2004). Inactivation of the Wip1 phosphatase inhibits mammary tumorigenesis through p38 MAPK-mediated activation of the p16(Ink4a)-p19(Arf) pathway. Nat. Genet. 36, 343–350.

Buschbeck, M., Uribesalgo, I., Wibowo, I., Rué, P., Martin, D., Gutierrez, A., Morey, L., Guigó, R., López-Schier, H., and Di Croce, L. (2009). The histone variant macroH2A is an epigenetic regulator of key developmental genes. Nat. Struct. Mol. Biol. 16, 1074–1079.

Cantariño, N., Douet, J., and Buschbeck, M. (2013). MacroH2A–an epigenetic regulator of cancer. Cancer Lett. 336, 247–252.

Chew, J., Biswas, S., Shreeram, S., Humaidi, M., Wong, E.T., Dhillon, M.K., Teo, H., Hazra, A., Fang, C.C., Lopez-Collazo, E., et al. (2009). WIP1 phosphatase is a negative regulator of NF-kappaB signalling. Nat. Cell Biol. 11, 659–666.

Colaprico, A., Silva, T.C., Olsen, C., Garofano, L., Cava, C., Garolini, D., Sabedot, T.S., Malta, T.M., Pagnotta, S.M., Castiglioni, I., et al. (2016). TCGAbiolinks: an R/Bioconductor package for integrative analysis of TCGA data. Nucleic Acids Res. 44, e71.

Creppe, C., Posavec, M., Douet, J., and Buschbeck, M. (2012). MacroH2A in stem cells: a story beyond gene repression. Epigenomics 4, 221–227.

Das, B., Tsuchida, R., Malkin, D., Koren, G., Baruchel, S., and Yeger, H. (2008). Hypoxia enhances tumor stemness by increasing the invasive and tumorigenic side population fraction. Stem Cells 26, 1818–1830.

Emelyanov, A., Gao, Y., Naqvi, N.I., and Parinov, S. (2006). Trans-kingdom transposition of the maize dissociation element. Genetics 174, 1095–1104.

Eppert, K., Takenaka, K., Lechman, E.R., Waldron, L., Nilsson, B., van Galen, P., Metzeler, K.H., Poeppl, A., Ling, V., Beyene, J., et al. (2011). Stem cell gene expression programs influence clinical outcome in human leukemia. Nat. Med. 17, 1086–1093.

Filipponi, D., Muller, J., Emelyanov, A., and Bulavin, D.V. (2013). Wip1 controls global heterochromatin silencing via ATM/BRCA1-dependent DNA methylation. Cancer Cell 24, 528–541.

Gentles, A.J., Plevritis, S.K., Majeti, R., and Alizadeh, A.A. (2010). Association of a leukemic stem cell gene expression signature with clinical outcomes in acute myeloid leukemia. JAMA 304, 2706–2715.

Grasset, E.M., Bertero, T., Bozec, A., Friard, J., Bourget, I., Pisano, S., Lecacheur, M., Maiel, M., Bailleux, C., Emelyanov, A., et al. (2018). Matrix stiffening and EGFR cooperate to promote the collective invasion of cancer cells. Cancer Res. 78, 5229–5242.

Gwak, J.M., Kim, M., Kim, H.J., Jang, M.H., and Park, S.Y. (2017). Expression of embryonal stem cell transcription factors in breast cancer: Oct4 as an indicator for poor clinical outcome and tamoxifen resistance. Oncotarget 8, 36305–36318.

Halazonetis, T.D., Gorgoulis, V.G., and Bartek, J. (2008). An oncogene-induced DNA damage model for cancer development. Science 319, 1352–1355.

Harada, H., Inoue, M., Itasaka, S., Hirota, K., Morinibu, A., Shinomiya, K., Zeng, L., Ou, G., Zhu, Y., Yoshimura, M., et al. (2012). Cancer cells that survive radiation therapy acquire HIF-1 activity and translocate towards tumour blood vessels. Nat. Commun. 3, 783.

Hochedlinger, K., Yamada, Y., Beard, C., and Jaenisch, R. (2005). Ectopic expression of Oct-4 blocks progenitor-cell differentiation and causes dysplasia in epithelial tissues. Cell 121, 465–477.

Hu, X., Ghisolfi, L., Keates, A.C., Zhang, J., Xiang, S., Lee, D.K., and Li, C.J. (2012). Induction of cancer cell stemness by chemotherapy. Cell Cycle 11, 2691–2698.

Kelly, P.N., Dakic, A., Adams, J.M., Nutt, S.L., and Strasser, A. (2007). Tumor growth need not be driven by rare cancer stem cells. Science 317, 337.

Kumar, S.M., Liu, S., Lu, H., Zhang, H., Zhang, P.J., Gimotty, P.A., Guerra, M., Guo, W., and Xu, X. (2012). Acquired cancer stem cell phenotypes through Oct4-mediated dedifferentiation. Oncogene 31, 4898–4911.

Lagadec, C., and Pajonk, F. (2012). Catch-22: does breast cancer radiotherapy have negative impacts too? Future Oncol. 8, 643–645.

Le Bin, G.C., Muñoz-Descalzo, S., Kurowski, A., Leitch, H., Lou, X., Mansfield, W., Etienne-Dumeau, C., Grabole, N., Mulas, C., Niwa, H., et al. (2014). Oct4 is required for lineage priming in the developing inner cell mass of the mouse blastocyst. Development 141, 1001–1010.

Lengner, C.J., Camargo, F.D., Hochedlinger, K., Welstead, G.G., Zaidi, S., Gokhale, S., Scholer, H.R., Tomilin, A., and Jaenisch, R. (2007). Oct4 expression is not required for mouse somatic stem cell self-renewal. Cell Stem Cell 1, 403–415.

Livyatan, I., Aaronson, Y., Gokhman, D., Ashkenazi, R., and Meshorer, E. (2015). BindDB: an integrated database and webtool platform for "reverse-ChIP" epigenomic analysis. Cell Stem Cell 17, 647–648.

Magee, J.A., Piskounova, E., and Morrison, S.J. (2012). Cancer stem cells: impact, heterogeneity, and uncertainty. Cancer Cell 21, 283–296.

Meacham, C.E., and Morrison, S.J. (2013). Tumour heterogeneity and cancer cell plasticity. Nature 501, 328–337.

Murakami, S., Ninomiya, W., Sakamoto, E., Shibata, T., Akiyama, H., and Tashiro, F. (2015). SRY and OCT4 are required for the acquisition of cancer stem cell-like properties and are potential differentiation therapy targets. Stem Cells 33, 2652–2663.

Naito, Y., Hino, K., Bono, H., and Ui-Tei, K. (2015). CRISPRdirect: software for designing CRISPR/Cas guide RNA with reduced off-target sites. Bioinformatics 31, 1120–1123.

Nordhoff, V., Hübner, K., Bauer, A., Orlova, I., Malapetsa, A., and Schöler, H.R. (2001). Comparative analysis of human, bovine, and murine Oct-4 upstream promoter sequences. Mamm. Genome 12, 309–317.

Nowell, P.C. (1976). The clonal evolution of tumor cell populations. Science 194, 23–28.

Parinov, S., Kondrichin, I., Korzh, V., and Emelyanov, A. (2004). Tol2 transposon-mediated enhancer trap to identify developmentally regulated zebrafish genes in vivo. Dev. Dyn. 231, 449–459.

Reddy, J.P., Peddibhotla, S., Bu, W., Zhao, J., Haricharan, S., Du, Y.C., Podsypanina, K., Rosen, J.M., Donehower, L.A., and Li, Y. (2010). Defining the ATM-mediated barrier to tumorigenesis in somatic mammary cells following ErbB2 activation. Proc. Natl. Acad. Sci. USA 107, 3728–3733.

Santos, M.A., Faryabi, R.B., Ergen, A.V., Day, A.M., Malhowski, A., Canela, A., Onozawa, M., Lee, J.E., Callen, E., Gutierrez-Martinez, P., et al. (2014). DNA-damage-induced differentiation of leukaemic cells as an anti-cancer barrier. Nature 514, 107–111.

Schmitt, C.A., McCurrach, M.E., de Stanchina, E., Wallace-Brodeur, R.R., and Lowe, S.W. (1999). INK4a/ARF mutations accelerate lymphomagenesis and promote chemoresistance by disabling p53. Genes Dev. 13, 2670–2677.

Schneider, C.A., Rasband, W.S., and Eliceiri, K.W. (2012). NIH Image to ImageJ: 25 years of image analysis. Nat. Methods 9, 671–675.

Shaffer, S.M., Dunagin, M.C., Torborg, S.R., Torre, E.A., Emert, B., Krepler, C., Beqiri, M., Sproesser, K., Brafford, P.A., Xiao, M., et al. (2017). Rare cell variability and drug-induced reprogramming as a mode of cancer drug resistance. Nature 546, 431–435.

Shreeram, S., Demidov, O.N., Hee, W.K., Yamaguchi, H., Onishi, N., Kek, C., Timofeev, O.N., Dudgeon, C., Fornace, A.J., Anderson, C.W., et al. (2006a). Wip1 phosphatase modulates ATM-dependent signaling pathways. Mol. Cell 23, 757–764.

Shreeram, S., Hee, W.K., Demidov, O.N., Kek, C., Yamaguchi, H., Fornace, A.J., Jr., Anderson, C.W., Appella, E., and Bulavin, D.V. (2006b). Regulation of ATM/p53-dependent suppression of myc-induced lymphomas by Wip1 phosphatase. J. Exp. Med. 203, 2793–2799.

Sporn, J.C., Kustatscher, G., Hothorn, T., Collado, M., Serrano, M., Muley, T., Schnabel, P., and Ladurner, A.G. (2009). Histone macroH2A isoforms predict the risk of lung cancer recurrence. Oncogene 28, 3423–3428.

Stracker, T.H., Roig, I., Knobel, P.A., and Marjanović, M. (2013). The ATM signaling network in development and disease. Front. Genet. 4, 37.

Takahashi, K., and Yamanaka, S. (2006). Induction of pluripotent stem cells from mouse embryonic and adult fibroblast cultures by defined factors. Cell 126, 663–676.

Visvader, J.E., and Lindeman, G.J. (2012). Cancer stem cells: current status and evolving complexities. Cell Stem Cell 10, 717–728.

Weber, M., Davies, J.J., Wittig, D., Oakeley, E.J., Haase, M., Lam, W.L., and Schubeler, D. (2005). Chromosome-wide and promoter-specific analyses identify sites of differential DNA methylation in normal and transformed human cells. Nat. Genet. 37, 853–862.

Withers, H.R., Maciejewski, B., Taylor, J.M., and Hliniak, A. (1988). Accelerated repopulation in head and neck cancer. Front. Radiat. Ther. Oncol. 22, 105–110.

CellPress

STAR★METHODS

KEY RESOURCES TABLE

REAGENT or RESOURCE	SOURCE	IDENTIFIER
Antibodies		
Anti-Histone H3 antibody - Nuclear Loading Control and ChIP Grade Polyclonal Antibody.	Abcam	Cat# ab1791; RRID: AB_302613
Rabbit Anti-Histone H3, trimethyl (Lys9) ChIP Grade Polyclonal Antibody.	Abcam	Cat# ab8898; RRID: AB_306848
Anti-acetyl-Histone H4 Polyclonal Antibody.	EMD Millipore	Cat# 06-598, RRID: AB_2295074
Rabbit Anti-Histone H3, acetyl (Lys 9) Polyclonal Antibody.	EMD Millipore	Cat# 07-352, RRID: AB_310544
Histone H3 (tri methyl K27 [mAbcam 6002] - ChIP Grade Monoclonal Antibody.	Abcam	Cat# ab6002, RRID: AB_305237
Dnmt1 [60B1220.1] - ChIP Grade Monoclonal Antibody.	Abcam	Cat# ab13537, RRID: AB_300438
Rabbit Anti-Rat macroH2A.1 Polyclonal Antibody.	Abcam	Cat# ab37264, RRID: AB_883064
Mouse Anti-Dnmt3b Monoclonal Antibody, Unconjugated, Clone 52A1018	Abcam	Cat# ab13604, RRID: AB_300494
Oct4 antibody - ChIP Grade	Abcam	Cat# ab19857, RRID: AB_445175
c-Myc antibody [8] - ChIP Grade	Abcam	Cat# ab17355, RRID: AB_443829
Mouse Anti-Human BRCA1 (D-9) Monoclonal, Unconjugated, Clone D-9 antibody	Santa Cruz Biotechnology	Cat# sc-6954, RRID: AB_626761
Anti-phospho-ATM (Ser1981), clone 10H11.E12 antibody	Millipore	Cat# 05-740, RRID: AB_309954
Rabbit Anti-Histone H2A.X, phospho (Ser139) Monoclonal Antibody, Unconjugated, Clone 20E3	Cell Signaling Technology	Cat# 9718, RRID: AB_2118009
5-Methylcytidine antibody	33D3, Isotype IgG1	Bio-Rad	Cat# MCA2201, RRID: AB_387479
Anti-5-methylcytosine (5-mC) antibody [33D3]	Abcam	Cat# ab10805, RRID: AB_442823
Anti-SIRT1 antibody	Abcam	Cat# ab 28170
Anti-acetyl-Histone H4 (Lys16) Antibody	Merck	Cat# 07-329, RRID: AB_310525
Chemicals, Peptides, and Recombinant Proteins		
ATM inhibitor KU55933	Selleckchem	S1092
Cyclophosphamide	Sigma	C0768-1G
Resveratrol	Enzo Liftech	BML-FR104-0500
Cisplatin	Hospital Pasteur CHU, Nice, FRANCE	N/A
SMARTpool: ON-TARGETplus BRCA1 siRNA	Dharmacon	L-003461
SMARTpool: ON-TARGETplus macroH2A.1 (H2AFY) siRNA	Dharmacon	L-011964-00-0005
Fluorescein-NAD and Cell Permeabilization Solution	Trevigen	4673-500-01
Wip1 inhibitor GSK2830371	Selleckchem	S7573
Flavopiridol (Alvocidib)	Selleckchem	S1230
(Z)-4 Hydroxytamoxifen	Sigma	H 7904-25MG
Xgal 40mg/ml	Euromedex	UX-1000-05-A
PARP inhibitor NU1025	Axon Medchem	Axon 1370
Proteinase K	Sigma	P2308

(Continued on next page)

Continued

REAGENT or RESOURCE	SOURCE	IDENTIFIER
RNase A	Promega	A797C
pGEM_T Easy Vector Systems	Promega	A1360
Restriction Enzymes, T4Ligase	New England Biolabs	
Q5 Hot Start High-Fidelity DNA Polymerase	New England Biolabs	M0493L
Subcloning Efficiency DH5α Competent Cells	Thermo Fisher Scientific	18265017
Puromycin	InVivoGen	ant-pr-1
Blasticidin	InVivoGen	ant-bl-05
Corning® Matrigel® Matrix (GFR)	Corning	354230
Rneasy free Dnase set	QIAGEN	79254
RevertedAid First Strand cDNA Synthesis kit	Thermo Fisher Scientific	K1622
Dynabeads protein G	Thermo Fisher Scientific	10003D
Dynabeads protein A	Thermo Fisher Scientific	10002D
Dynabeads M-280 Sheep anti-mouse IgG	Thermo Fisher Scientific	11201D
Power Syber Green Cell-to-CT	Ambion	4402954
Complete Mini EDTA-free	Roche	11836170001
PhosSTOP	Roche	04906837001
Critical Commercial Assays		
KAPA SYBR FAST qPCR Kit	Merck	KK4602
KIT FOR ARRAY		
RNeasy Mini Kit	QIAGEN	74104
DNeasy Blood & Tissue Kits	QIAGEN	69506
QIAquick PCR Purification Kit	QIAGEN	28104
PureYieldTM Plasmid Miniprep System	Promega	A1222
Neon Transfection System 100 μL Kit	Thermo Fisher Scientific	MPK10025
Deposited Data		
MICROARRAY	NCBI	GSE99796
Raw fluorescent images	Mendeley	https://doi.org/10.17632/r83y448z5j.1
Experimental Models: Cell Lines		
HCT116	ATCC	ATCC® CCL-247
MCF7	ATCC	ATCC® HTB22™
T27	(Brichkina et al., 2016)	N/A
HN30	(Grasset et al., 2018)	N/A
HEK293T	ATCC	ATCC® CRL-3216
Experimental Models: Organisms/Strains		
Mus musculus: Strain background: mixed		
Eμ-myc transgene mice	(Shreeram et al., 2006b)	N/A
Oct4 CreERT2: (Tg(Pou5f1-cre/ERT2)#Ysa)	Jackson Laboratory	MGI: 5615471
Rosa26-LacZ: (B6;129S-*Gt(ROSA)26Sor*/J)	Jackson Laboratory	002073
Oct4$^{LoxP/LoxP}$	(Le Bin et al., 2014)	N/A
Rosa26-CreERT2	(Le Bin et al., 2014)	N/A
NOD.Cg-*Prkd^{cscid} Il2rg^{tm1Wjl}*/SzJ	Jackson Laboratory	005557
Oligonucleotides Primers for qRT-PCR		
hOCT4A	FOR	CGCAAGCCCTCATTTCAC
hOCT4A	REV	CATCACCTCCACCACCTG
hOCT4B	FOR	CAGGGAATGGGTGAATGAC
hOCT4B	REV	AGGCAGAAGACTTGTAAGAAC
hOCT4B1	REV	TCCCTCTCCCTACTCCTCTTCA

(Continued on next page)

CellPress

Continued

REAGENT or RESOURCE	SOURCE	IDENTIFIER
hOCT4B1	FOR	GGG TTC TATTTGGTGGGTTCC
hNANOG	FOR	ATTCAGGACAGCCCTGATTCTTC
hNANOG	REV	TTTTTGCGACACTCTTCTCTGC
hSOX2	FOR	TACAGCATGTCCTACTCGCAG
hSOX2	REV	GAGGAAGAGGTAACCACAGGG
hKLF4	FOR	TCCCATCTTTCTCCACGTTC
hKLF4	REV	GGTCTCTCTCCGAGGTAGGG
h c-MYC	FOR	AATGAAAAGGCCCCCAAGGTAGTTATCC
h c-MYC	REV	GTCGTTTCCGCAACAAGTCCTCTTC
h18S	FOR	AACTAAGAACGGCCATGCAC
h18S	REV	CCTGCGGCTTAATTTGACTC
hGAPDH	FOR	CCATGACCCCTTCATTGACC
hGAPDH	REV	GACAAGCTTCCCGTTCTCAG
hFAS	FOR	TTGCAGAAGGAGCTCACAGA
hFAS	REV	GAGGTCAGAAGACCCTGTGG
hCCNG2	FOR	GCTGAATGTGGGTGTATCCTC
hCCNG2	REV	CCAAAACCTCGTGGCTTAAA
hGADD45a	FOR	GAACCATGCAGGAAGGAAAA
hGADD45a	REV	CCAAACTATGGCTGCACACTT
hSESN1	FOR	GGCAGCTGTCTTGTGCATTA
hSESN1	REV	AGGCAGAGGCAGAGAGACTG
hSESN2	FOR	GGTGTGCAGGAGAGAAGAGG
hSESN2	REV	GCAAAGCCAAAGATTTCTGC
hp16	FOR	GAAGGTCCCTCAGACATCCC
hp16	REV	CCCTGTAGGACCTTCGGTGA
hLGR5	FOR	GGTTCAGTAACATTAAGGACCATGA
hLGR5	REV	GAAAATGGGCAGAGAAACACA
hSNAI2	REV	TGTTGCAGTGAGGGCAAGAA
hSNAI2	FOR	GACCCTGGTTGCTTCAAGGA
hHEY1	FOR	CCTGGGACTGCCATATTTTC
hHEY1	REV	TCAAAGAGAAGGAGGCAGGA
hMSX2	FOR	GGCAGAAGGTAAAGCCATGT
hMSX2	REV	GGACAGATGGACAGGAAGGT
hBRCA1	FOR	GCATCTGGGTGTGAGAGTGA
hBRCA1	REV	AGTTCAGCCATTTCCTGCTG
hDNMT3B	FOR	GAGTCCCCCGTGGAGTTC
hDNMT3B	REV	TAGGGGGTACTGCTGCTCTG
hmacroH2A.1	FOR	CCGCCGTCCTGGAATACC
hmacroH2A.1	REV	GTTGTCTCTCGCTGCATTGC
hb-tubulin	FOR	GCGAGATGTACGAAGACGAC
hb-tubulin	REV	TTTAGACACTGCTGGCTTCG
hATM	FOR	TTGATCTTGTGCCTTGGCTAC
hATM	REV	TATGGTGTACGTTCCCCATGT
hATR	FOR	ACCTCAGCAGTAATAGTGATGGA
hATR	REV	GGCCACTGTATTCAAGGGAAAT
ChIP and MeDIP qPCR		
A OCT4	FOR	AGGAGTCTAGGCATGCAGGA	MeDIP
A OCT4	REV	AAACACCTTCCCCAATTTCC	MeDIP

(Continued on next page)

CellPress

Continued

REAGENT or RESOURCE			SOURCE	IDENTIFIER
B OCT4	FOR	AAGAGGGTGGTGTTGAGTGG	MeDIP	ChIP
B OCT4	REV	GCTGGAATCTCCACACCAGT	MeDIP	ChIP
C OCT4	FOR	GTGATGGTTCTGTCCTGGGG	MeDIP	
C OCT4	REV	CTCTGTTCGTGTGCCCATCT	MeDIP	
D OCT4	FOR	GCAGATAGAGCCACTGACCC	MeDIP	
D OCT4	REV	CATGCTGCTGGTCTAGTGCT	MeDIP	
E OCT4	FOR	TCAAGCACTAGACCAGCAGC	MeDIP	
E OCT4	REV	AGTTCCTCCTTCCTCTGGGG	MeDIP	
F OCT4	FOR	TTTGAGGGGATTGCAGAGGG	MeDIP	
F OCT4	REV	CAAAGAAGCCTGGGAGGGAC	MeDIP	
G OCT4	FOR	CCATCCAGGCCCATTCAAGG	MeDIP	ChIP
G OCT4	REV	ACATCAGGTTCCTTGCTCCC	MeDIP	ChIP
H OCT4	FOR	AGCAAGGAACCTGATGTGCA	MeDIP	
H OCT4	REV	CAGCCTGCCAAATTTCACCC	MeDIP	
I OCT4	FOR	GATCGGGGGAAGGCATAAGG	MeDIP	
I OCT4	REV	GGAATCACTCCCACACCTCC	MeDIP	
L OCT4	FOR	GCACCTGGGTTCCTGAAGAA	MeDIP	
L OCT4	REV	TCTGCTCCAGCCTCCTAAGT	MeDIP	
M OCT4	FOR	TGCTTTGGCCCAGTAGATCG	MeDIP	ChIP
M OCT4	REV	CACTAGCCTTGACCTCTGGC	MeDIP	ChIP
N OCT4	FOR	GCCACCACCATTAGGCAAAC	MeDIP	
N OCT4	REV	AAATCCGAAGCCAGGTGTCC	MeDIP	
O OCT4	FOR	CAACCTAACCCTGGCCTCAG	MeDIP	
O OCT4	REV	ATTAACAGGCATGCGTCACCA	MeDIP	
P OCT4	FOR	TTAAAAGGTGTGGCCAGGCA	MeDIP	
P OCT4	REV	GATCTGTCCACCTTGGCCTC	MeDIP	
Q OCT4	FOR	TGACGCATGCCTGTAATCTC	MeDIP	ChIP
Q OCT4	REV	TTTGTTGCCTAGGCTGGAGT	MeDIP	ChIP
hNANOG promoter	FOR	TGAATGTTGGGTTTGGGAAT	MeDIP	ChIP
hNANOG promoter	REV	GCTTTTTCCCTCTGGCTCTT	MeDIP	ChIP
hH19ICR-F	FOR	GAGCCGCACCAGATCTTCAG	MeDIP	
hH19ICR-R	REV	TTGGTGGAACACACTGTGATCA	MeDIP	
hUBE2B-F	FOR	CTCAGGGGTGGATTGTTGAC	MeDIP	
hUBE2B-R	REV	TGTGGATTCAAAGACCACGA	MeDIP	
A SOX2	FOR	GGCTTTGTTTGACTCCGTGT	MeDIP	
A SOX2	REV	ATTTTAGCCGCTCTCCCATT	MeDIP	
B SOX2	FOR	CCCCCTTTCATGCAAAAC	MeDIP	
B SOX2	REV	GGGTTTCTAGCGACCAATCA	MeDIP	
C SOX2	FOR	GAGGAGGGAAGCGCTTTTT	MeDIP	
C SOX2	REV	GAGGAAAATCAGGCGAAGAA	MeDIP	
D SOX2	FOR	ATGATGGAGACGGAGCTGAA	MeDIP	
D SOX2	REV	GGGCTGTTTTTCTGGTTGC	MeDIP	
p16	FOR	AGCACTCGCTCACGGCGTC		ChIP
p16	REV	CTGTCCCTCAAATCCTCTGGAG		ChIP
hOCT4 promoter	FOR	AGTCTGGGCAACAAAGTGAGA		ChIP
hOCT4 promoter	REV	AGAAACTGAGGCGAAGGATG		ChIP
hOCT4 distal enhancer	FOR	AGGGCTCAGTCCTTCAACCT		ChIP
hOCT4 distal enhancer	REV	AAAACGCGGTAGTCATCTGG		ChIP

(Continued on next page)

CellPress

Continued

REAGENT or RESOURCE	SOURCE	IDENTIFIER
Recombinant DNA		
psPAX2	Addgene	12260
pMD2.G	Addgene	12259
pLV.ATMi	Addgene	14542
pLL-hOCT4i −1	Addgene	12198
pLL-hOCT4i −2	Addgene	12197
hCas9	Addgene	41815
gRNA_Cloning Vector	Addgene	41824
DS transposon and AcTransposase	(Emelyanov et al., 2006)	NA
Tol2 transposon and Tol2 transposase	(Parinov et al., 2004)	NA
pMXs-hOCT3/4	Addgene	17217
pMXs-hSOX2	Addgene	17218
pMXs-hSOX2	Addgene	17220
pMXs-hKLF4	Addgene	17219
ptetO-GATA4	Addgene	46003
pcDNA3/Myc-DNMT3B1	Addgene	35522
pLentiWIP1sh-GFP plasmids	(Shreeram et al., 2006a)	NA
Software and Algorithms		
ImageJ (version 1.48k)	(Schneider et al., 2012)	https://imagej.nih.gov/ij/index.html
GraphPad Prizm program		https://www.graphpad.com/scientific-software/prism/
TCGAbiolinks v2.7.3 package in R		
suvival package v2.41-3 in R		
survminer package v0.41 in R		

CONTACT FOR REAGENT AND RESOURCE SHARING

Further information and requests for resources and reagents should be directed to the lead contact, Dmitry V. Bulavin (Dmitry.Bulavin@unice.fr).

EXPERIMENTAL MODEL AND SUBJECT DETAILS

Animal Experimentation

WIP1 deficient mice and eμ-myc transgene are previously described (Shreeram et al., 2006b). Oct4 CreERT2 and Rosa26-LacZ mice were purchased from the Jackson Laboratory. Oct4$^{LoxP/LoxP}$, and Rosa26-CreERT2 mice are previously described (Le Bin et al., 2014). Mice were checked for tumors twice a week by palpation. For relapse experiments, lymphoma-containing mice were injected with a single dose of 300mg/kg cyclophosphamide as previously described (Schmitt et al., 1999). One week later, mice were analyzed for tumors by palpation and considered as day "0" if not tumor was found.

For lineage tracing analysis primary or relapsed lymphoma were collected, washed twice in cold ice and fixed in 0,5% glutaraldehyde/2% PFA and stained with 1mg/ml X-gal at 37°C for 4-6h.

For lung tumor cells graft experiments orthotropic xenograft were performed by tail-vein intravenous injection of 1-2,5X10^5 tumor T27 cells in 100 μL PBS in NSG mice. Mice were sacrificed 3 weeks after injection, and lung were observed under fluorescent microscope.

Head and Neck tumor xenotropic experiments were performed by subcutaneous injection of 2,5X10^5 HN30 tumor cells in 50% Matrigel in lower flanks of NSG mice. Tumor growth was monitored by palpation once a week, and animals were sacrificed when tumor size reached 1cm^3. Tumors were excised and observed under fluorescent microscope or used for other analysis. The cisplatin injection was performed 5 days after tumor cells grafting at 5 μg/g mice.

All animal experiments were performed in compliance with the Animal Care and Use Committee and approved by the ethical review committee CIEPAL D'AZUR.

METHOD DETAILS

Cell Culture and treatments

HCT116 and MCF7 cells were maintained as monolayers in DMEM and RPMI 1640 respectively supplemented with 10% heat-inactivated fetal calf serum, 2mM glutamine and 0.6% Pen-Strep at 37°C in a 5% CO_2 atmosphere. For low oxygen experiments cells were maintained in a 5% O_2 incubator for 12 days. Chemo-drug treatment was performed with cyclophosphamide (Harada et al., 2012) or with 1ng/ml cisplatin. Cultured HCT116 and MCF7 parental cells parental were infected with retrovirus targeting human WIP1 (Chew et al., 2009) to generate WIP1 SH HCT116 and WIP1 SH MCF7 cell lines. Sphere cell culture was performed in low-attachment plate in DMEM-F12 supplemented with 4% BSA, 0.6% Pen-Strep, B27, 20ng/ml bFGF, 20ng/ml EGF and insulin at 37°C in a 5% CO_2 atmosphere. Medium was replaced every 2 days.

For transient overexpression experiments cultured WIP1-depleted HCT116 and parental cell lines were electroporated with plasmids expressing DNMT3B, MYC, OCT4, SOX2, KLF4 and GATA4 using NEONTH transfection system (Invitrogen) according to manufacturing instruction protocol. 72h post transfection cells were harvested and processed for mRNA and/or DNA methylation analysis. For siRNA experiments, HCT116 and MCF7 cells were transfected with a pool of 4 siRNAs at 10nnm final concentration (Dharmacon) for each individual gene according Dharmacon instruction protocol. 48 or 72h post transfection, cells were harvested and processed for RNA, DNA methylation and ChIP analysis. Chemical inhibition of parental lines was performed with 10 μM WIP1 inhibitor and with 10 μM PARP inhibitor KU1025. Chemical treatment of Wip1 SH HCT116 was performed with 10 μM ATM inhibitor KU55933, (ChemDiv, USA) for three days and Flavopiridol (Selleckchem) for 6h.

Patient tumor material was collected in culture medium and partially digested for 1 hour at room temperature in RPMI1640 with 1 mg/ml Collagenase IV, 1 mg/ml Dispase and 1mg/ml Hyalouronidase. Single cancer cell suspensions used for further analysis.

Labeling of live cells for activation of DNA damage signaling

This protocol is based on the analysis of ability to build long PAR chains by NAD-consuming enzymes poly (ADP-ribose) polymerases (e.g., PARP-1, PARP-2). PARPs are rapidly and robustly activated by DNA damage signaling resulting in utilization of NAD to produce long PAR chains. When Fluorescein-conjugated NAD is used, after incorporation into long PAR chains, FITC is covalently bound and thus retained in a cell. This in turn produces a strong fluorescent signal. In brief, cells are incubated for 10min on ice in 50 mM HEPES, pH 7.4 containing 140mM NaCl, 1mM DTT, 100 uM 6-Fluo-10NAD$^+$ (Biolog Life Science Institute). We used 50 uM Cell Permeabilization Solution (Trevigen, cat# 4674-250-01) to allow for the efficient transfer of Fluorescein-conjugated NAD across cellular membranes in live cells. Subsequently, cells were washed 3 times with cold PBS and used for FACS-sorting for subsequent analysis. Chemical treatment of parental cell line was performed with 10 μM ATM inhibitor KU55933, (ChemDiv, USA) and with 10 μM PARP inhibitor KU1025. Cell Permeabilization reagent has been discontinued but could be replaced by an alternative reagent, please contact the authors for more details.

Immunofluorescence

For immunofluorescent analysis, cells were fixed 10min in 4% paraformaldehyde, washed three times in PBS 0.1% BSA and permeabilized with 0.1% Triton for 10min. After washing cells were blocked in 5% BSA for two hours and incubated with the respective primary antibody: overnight a 4°C for mouse anti-phospho-S1981 pATM (1:150,) and 2h at room temperature for p-Histone H2A.X S139 (1:300) and OCT4A (1:200). After washing, secondary antibodies were added for 1 hour at room temperature. The slides were washed and mounted into the Mounting Medium with DAPI (Vector Laboratories). All slides were analyzed using confocal microscopy.

Chromatin Immunoprecipitation

Chromatin immune-precipitation was prepared in accordance with the Upstate Biotechnology and Abcam protocol, with some modifications. Cells were fixed at room temperature by addition of 1% formaldehyde for 10 min. Fixation was stopped by addition of 0.125 M glycine. Cells were washed three times in PBS, re-suspended in SDS buffer (50 mM Tris at pH 8.1, 0.5% SDS, 100 mM NaCl, 5 mM EDTA, protease inhibitors and phosphatase inhibitors) and stored at −80°C or directly shared by sonication and processed for ChIP. For histone marks, lysates were immunoprecipitated with 3 to 5 μg of the corresponding antibody pre-bound to A- or G-protein coupled paramagnetic beads (Dynabeads) in PBS/BSA 0.5%. For all proteins analyzed lysate were immunoprecipitated with 10 μg of the corresponding antibody. After overnight incubation beads were washed 6 times in a modified RIPA buffer (50 mM HEPES pH 7.6, 500 mM LiCl, 1 mM EDTA, 1% NP-40, 0.7% Na-deoxycholate) and once in TE containing 50 mM NaCl. DNA was eluted in TE/2% SDS and crosslink reversed by incubation overnight at 65°C. DNA was then purified by Qiaquick columns (QIAGEN) and quantified using qPCR analysis. Duplicate immunoprecipitations experiments were performed with protein A/G-agarose beads (Invitrogen) or Dynabeads Protein A/G (Life Technologies) and respective antibodies. Input and immunoprecipitated samples were analyzed by qRT-PCR with respective primers. The relative enrichment of each marker was calculated as the ratio between the net intensity of each bound sample divided by the input.

DNA Methylation Analysis

Methylated DNA immunoprecipitation was carried out in accordance with the protocol laid out by Weber et al., 2005. Purified genomic DNA was randomly sheared by sonication and precipitated with 400mM NaCl, two volumes of Ethanol 100% and 1ul of

glycogen. 5ul of 5meC antibody was incubated at 4°C with Dynabeads M-280 Sheep anti-mouse IgG for 4-6h. 2ug of sonicated DNA was denatured for 10 minutes at 100°C, immediately cool on ice for 10 minutes and incubated with Dyanabeads-antibody complex for 3h at 4°C with overhead shaking. Magnetic beads were washed 5 times with 1X washing buffer (10mM Na-Phosphate pH 7, 0.14M NaCl, 0,5% Triton X-100) and suspended in 100ul of proteinase K digestion buffer (50mM Tris-HCl pH8, 10mM EDTA, 0.5%SDS 7ul of proteinase K (10mg/ml)) and incubated 3h at 50°C. DNA was purified using PCR purification kit (QIAGENE) and MeDIP fraction was measured by qPCR. Starting material was normalized between different samples. Duplicate or triplicate immunoprecipitations experiments were performed with Dynabeads™ M-280 sheep anti-Mouse IgG (INVITROGEN) and anti-5meC antibody (Abcam and Bio-Rad). Input and immunoprecipitated samples were analyzed by SYBR Green qPCR with respective primers. The relative enrichment of each marker was calculated as the ratio between the net intensity of each bound sample divided by the input.

Gene Expression and Microarray Analysis
Total RNA was isolated using the RNeasy Mini Kit (QIAGEN) and treated with DNase (QIAGEN) in accordance with the manufacturer's instructions. 0.5 μg of total RNA was reverse transcribed using RevertAid First Strand cDNA Synthesis Kit (Thermo Scientific™). Alternatively, for low starting material, Power SYBER Green Cell-to-CT™ (AMBION) was used in accordance with manufacturer's instructions. Quantitative real-time PCR reactions were performed with the SYBER Green (KAPA Biosystem) in MicroAmp Optical 96-well plates using a StepOnePlus System (Applied Biosystems).

For microarray analysis: the expression data from triplicate Illumina Human microarrays using HumanHT-12 v4 Expression BeadChip Kit. log2 fold changes were computed and only transcripts with an absolute fold change greater than 1.4 fold, an intensity greater than 100 and a multiple testing adjusted p-value of less than 0.05 were labeled as significantly differentially expressed resulting in 300 down and 514 upregulated probe in WIP1-depleted HCT116 cells related to parental cell line. The microarray data was deposited in the Gene Expression Omnibus database with the accession number GSE99796.

CRISPR/Cas9-mediated knock-in of CreERT2 into human OCT4 locus and genetic lineage tracing
gRNA targeting 5th exon of POU5F1 at position Ch.6: 31164765 (GRCh38) was designed using CRISPRdirect program (http://crispr.dbcls.jp;(Naito et al., 2015)). Oligonucleotides O4gRNA7GF: TTTCTTGGCTTTATATATCTTGTGGAAAGGACGAAA CACCGGCTGGGTCTCCTTTCTCAG and O4gRNA7GR:

GACTAGCCTTATTTTAACTTGCTATTTCTAGCTCTAAAACCTGAGAAAGGAGACCCAGCC were used for cloning gRNA into gRNA cloning vector (Addgene #41824) via Gibson Assembly method to make pO4g7RNA.

To generate OCT4 targeting plasmid (pTargetO4g7), the cassette, containing F2ACreER^{T2}T2ATKP2AFP635 and PGK-puro was cloned in-frame with the fragments for homologous recombination. The amplified left (632 bp) and right (655 bp) homology arms were cloned into Pme/Xba and EcoRI/SnaB sites flanking Cre-Puro cassette. Primers for amplification: Left arm - O4LAFPme: AGATGTTTAAACCTCTGCTGACACATCTAGTCACAG / O4LA7RXba: AGAGTCTAGAAGAGAAAGGAGACCCAGCAGCCTC; right arm - O4RA7FEcoRI: AGAGGAATTCTTCTCAGGGGGACCAG / O4RA7RSnaB: AGAGTACGTAGCAAAAGTTCTTGCATCACAGG.

Cells were transfected with the mix of plasmids pTargetO4g7/phCas9 (Addgene #41815)/ pO4g7RNA with ratio 4:1:1 by electroporation using Neon Transfection System (Thermo Fisher Scientific) with 1130 v/30ms/2 pulses settings. The cell clones with recombination events were selected after 1 week growth with presence of 0,5 μg/ml puromycin. The reporter construct (pMTCMVLBsLTG) was cloned into Tol2 transposon backbone. The CMV driven floxed blasticidin-S deaminase was cloned in front of fluorescent protein TurboGreen. To generate cells with stable transfected reporter, OCT4 knock in cell lines were transfected with the mix of plasmids pMTCMVLBsLTG and pCMV-Tol2 Transposase at the ratio 4:1 by electroporation, and Blasticidin at 50-μg/ml selections during 1 week has been used to obtain clones with transposon integrations.

T27 Knock-in/Reporter cell line was infected with lentivirus, expressing shRNA against ATM (Addgene). Supernatant, containing lentivirus was generated by co-transfection HEK293T with mix plasmids pLV.ATMi/ psPAX2/ pMD2.G with ratio 2:1:0,5 and harvested after 48 and 72 hour post-transfection. Tumor cells were infected with supernatant in presence 8 μg/ml polybrene for 12 hours and selected with 2 μg/ml puromycin for 5 days

Bioinformatics analysis
Data from TCGA were downloaded using the TCGAbiolinks v2.7.3 package in R (Colaprico et al., 2016). Gene expression data as HTSeq upper quartile FPKM values and Illumina 450 array based methylation data as beta values were mapped to hg38. Due to unavailability of hg38-mapped data, isoform level RSEM TPM values for both myc isoforms were mapped to hg19. Only unique Primary Blood Derived Cancer and Primary Solid Tumor labeled samples were included and datasets with fewer then 10 patients per group were excluded from the analysis. Hazard ratios for POU5F1 methylation levels (beta) were estimated using a univariate Cox proportional hazards model and significance was assessed using the log rank test. Kaplan-Meier survival curves were calculated using the survfit command from the suvival package v2.41-3 in R. Trended, Andersen modified Peto-Peto p values to compare three, ordered Kaplan-meier survival curves were calculated using the survminer package v0.41 in R.

Statistical analysis

Values are means ± SD. Comparison of mean values between groups was evaluated by 2-tailed Student's t test using the GraphPad Prizm program. Statistical analysis of animal survival was carried out with the use of PRIZM software using log-rank (Mantel-Cox) test, longrank test for trend and Gehan-Breslow-Wilcoxon test. P values less than 0.05 were considered significant. Any P value less than 0.05 was designated with one (*) asterisk; less than 0.01 – with two (**) asterisks, less than 0.001 – with three (***) asterisks.

DATA AND SOFTWARE ACCESSIBILITY

All the original data for Immunofluorescence have been deposited with Mendeley and can be accessed with https://doi.org/10.17632/r83y448z5j.1.